SEDIMENTOLOGY the journal of the International Association of Sedimentologists

Sedimentology (2023) **70**, 1195–1223 doi: 10.1111/sed.13074

A terminal Messinian flooding of the Mediterranean evidenced by contouritic deposits on Sicily

GIJS VAN DIJK*, JASPER MAARS*, FEDERICO ANDREETTO*, F. JAVIER HERNÁNDEZ-MOLINA†, FRANCISCO J. RODRÍGUEZ-TOVAR‡ and WOUT KRIJGSMAN*

**Department of Earth Sciences, Utrecht University, Princetonlaan 8a, Utrecht, 3584 CB, The Netherlands (E-mail: gijsbertannevandijk@gmail.com)*

†Department of Earth Sciences, Royal Holloway University of London, Egham, Surrey, TW20 0EX, UK

‡Departamento de Estratigrafía y Paleontología, Universidad de Granada, Granada 18002, Spain

Associate Editor – Adam McArthur

ABSTRACT

The evolution of marine gateways and sea straits exerts major control on bottom current depositional systems. A well-known interval in geological history characterized by frequent changes in marine connectivity is the Messinian Salinity Crisis (5.97 to 5.33 Ma) when the Mediterranean allegedly experienced major (>1 km) sea-level drawdown followed by a catastrophic marine replenishment at the base of the Zanclean. Controversy exists around the timing and mode of this event as unambiguous flood deposits have so far never been drilled or recognized in outcrops. In the Sicilian Caltanissetta Basin (Italy), the Messinian/Zanclean boundary is directly underlain by the Arenazzolo Formation. This 5 to 7 m thick sandy sedimentary interval may reveal a genetic link with the abrupt refilling of the Mediterranean, but at present a detailed study to understand its origin is lacking. In this work, the Arenazzolo Formation at Eraclea Minoa has been studied by a multi-method approach, employing detailed facies description, grain-size analyses, petrographic analyses and palaeocurrent analyses. Palaeogeographical reconstructions and facies associations show that the Arenazzolo Formation sands were deposited on the northern flank of the Gela thrust front by persistent bottom currents, flowing parallel to the regional slope physiography, during a transgression. It is hypothesized that these currents are associated with the active circulation of surface and intermediate water masses coeval with a terminal Messinian flood, when basin margins overtopped and a reconnection between western and eastern Mediterranean was created. The Arenazzolo Formation is a unique example of a contouritic deposit formed by bottom currents that establish during the reconnection of major isolated water bodies.

Keywords Bottom currents, contourites, marine gateways, Messinian Salinity Crisis, Messinian/Zanclean boundary, Sicily Sill.

INTRODUCTION

During the late Messinian, major changes in intrabasinal and extrabasinal connectivity in the Mediterranean Sea led to a major drawdown of Mediterranean base-level and highly fluctuating salinities (Selli, 1960; Hsü, 1972; Hsü *et al.*, 1973; Krijgsman *et al.*, 1999; Roveri *et al.*, 2014). The so-called Messinian Salinity Crisis (MSC) was a short-lived ecological and environmental crisis, which caused the accumulation of more than a million cubic metres of salt on the

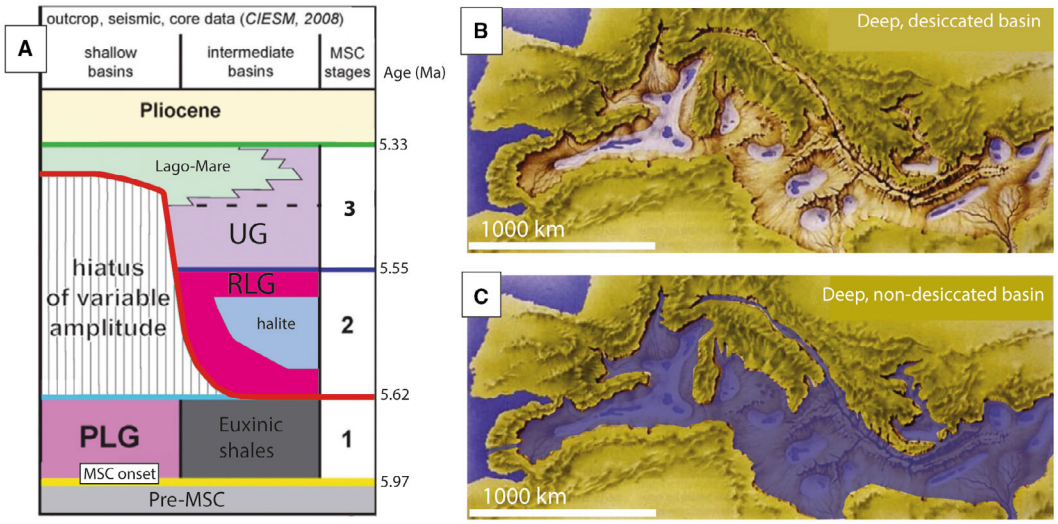

Fig. 1. (A) Three-fold stratigraphic scheme for the MSC, with a subdivision in three main stages (Roveri *et al.*, 2014). PLG, Primary Lower Gypsum; RLG, Resedimented Lower Gypsum; UG, Upper Gypsum. (B) Scenario of an isolated, lake-dotted Mediterranean during Stage 3. (C) Alternative scenario of an almost full and (at least partially) connected Mediterranean. (B) and (C) are modified after Attenborough (1987).

Mediterranean sea floor (Ryan, 2009; Haq *et al.*, 2020). The MSC is largely thought to have evolved in three stages (Roveri *et al.*, 2014, Fig. 1A): (i) Primary Lower Gypsum (PLG) deposition concentrated in shallow marginal basins (Lugli *et al.*, 2010) and possibly intermediate basins (Ochoa *et al.*, 2015; Raad *et al.*, 2021) during Stage 1 (5.97 to 5.59 Ma); (ii) maximum sea-level drawdown with halite precipitation in the deepest basins (5.59 to 5.55 Ma); and (iii) gypsum deposition alternating with brackish water marls in intermediate and deep basins (5.55 to 5.33 Ma). For this third phase (also termed Stage 3 or Lago-Mare) three competing palaeoenvironmental scenarios exist.

1 The Mediterranean was isolated and consisted of disconnected subbasins with continental and shallow endorheic lakes fed by local rivers (Rouchy *et al.*, 2001; Ryan, 2009; Caruso *et al.*, 2020, Fig. 1B).

2 The Mediterranean was almost full with interconnected subbasins and waters were at least temporarily Atlantic-fed (Vasiliev *et al.*, 2017; García-Veigas *et al.*, 2018; Andreetto *et al.*, 2021, Fig. 1C).

3 The Mediterranean was oscillating with high-amplitude precession-controlled base-level fluctuations (Rouchy & Caruso, 2006; Andreetto *et al.*, 2022a).

Scenarios 1 and 3 imply a significant bathymetric contrast between the Messinian and Zanclean and suggest a catastrophic end to the MSC with the collapse of the Gibraltar Sill, and the abrupt re-establishment of open marine conditions all over the Mediterranean at the beginning of the Zanclean (Hsü *et al.*, 1973; Garcia-Castellanos *et al.*, 2009; Amarathunga *et al.*, 2022).

The concept of a major bathymetric change at the end of the Messinian is supported by the observation of erosional and depositional morphologies, recorded in seismic data-sets from the deep Mediterranean (Garcia-Castellanos *et al.*, 2009, 2020; Micallef *et al.*, 2018; Spatola *et al.*, 2020). Incisions and chaotic flood deposits recognized in seismic profiles are interpreted as the expression of a Zanclean reflooding of the Mediterranean, reaching discharges possibly above 100 sverdrup (Sv) (Garcia-Castellanos *et al.*, 2009). Sandstones straddling the Messinian/Zanclean boundary at Ocean Drilling Program (ODP) sites 974 and 975 (Tyrrhenian and South Balearic Sea) are thought to be the result of suspension transport during this Zanclean Flood (Zahn *et al.*, 1999). Still, unambiguous observations of flood deposits in outcrops on land have not been documented and linked to the Mediterranean reflooding. Micallef *et al.* (2018) provide photographs of Zanclean breccias deposited on the Hyblean Plateau and presumes

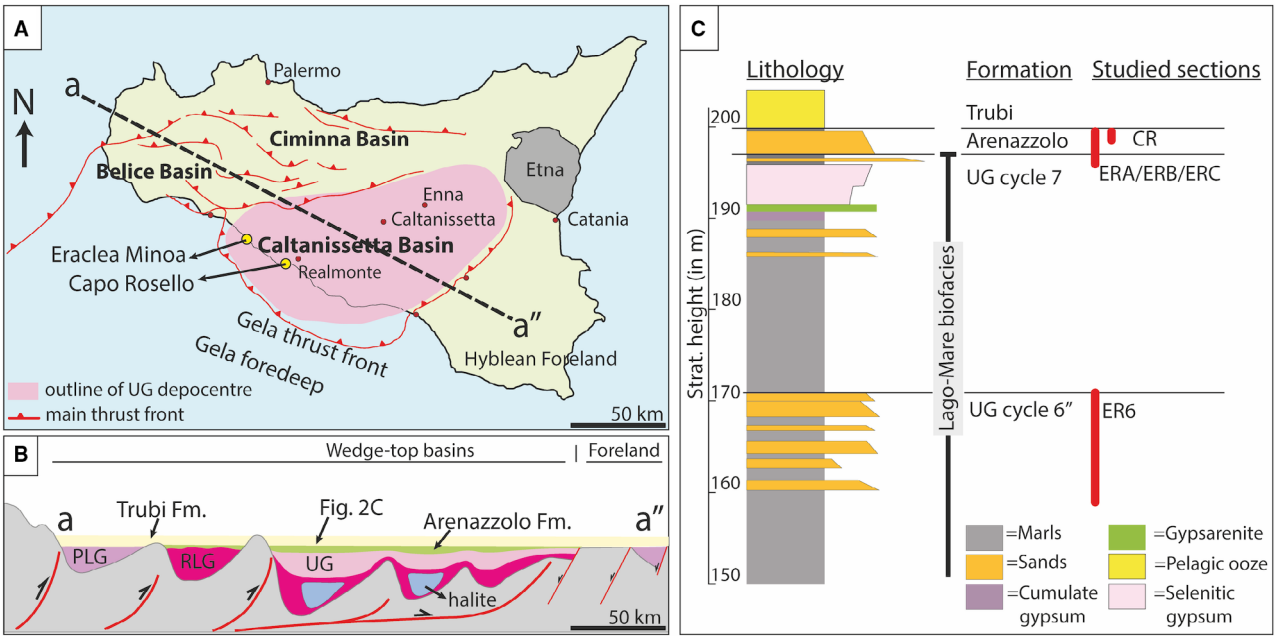

Fig. 2. (A) Simplified geological map of Sicily. (B) Schematic geological cross-section through Central Sicily, flattened at the Miocene–Pliocene boundary. Three Messinian units (PLG, Primary Lower Gypsum; RLG, Resedimented Lower Gypsum; UG, Upper Gypsum) correspond to the three stages depicted in Fig. 1A. (C) Stratigraphic log of the uppermost UG in Eraclea Minoa, indicating the intervals that were studied in detail (sections ERA/ERB/ERC/ER6/CR). All panels were modified after Manzi *et al.* (2009).

these are flood deposits, but description and interpretation of these facies is limited.

One of the best studied records of the Messinian to Zanclean transition in the Mediterranean is that of the Sicilian Caltanissetta Basin (Fig. 2A and B). It comprises the Messinian Upper Gypsum unit (UG), the uppermost Messinian Arenazzolo Formation and lowermost Zanclean Trubi Formation. The UG unit (corresponding to the third MSC phase) bears seven rhythmic couplets of primary gypsum beds, coarse terrigenous deposits and marls (Manzi *et al.*, 2009; Andreetto *et al.*, 2022a), of which the upper two are shown in Fig. 2C. The uppermost clays just above UG cycle 7 are overlain by a 5 to 7 m thick sandy to silty unit called the Arenazzolo Formation (Fig. 2C), located right below the basal Zanclean (Ogniben, 1957; Brolsma, 1978; Cita & Colombo, 1979). Sedimentological facies descriptions of the Arenazzolo Formation have never been dealt with in depth and a genetic link between these deposits and the Zanclean reflooding has never been proven. This study aims to construct a sedimentary model for the uppermost part of the UG and the Arenazzolo Formation at the Eraclea Minoa and Capo Rosello sections on Sicily and explores whether the Arenazzolo Formation could be the expression of the terminal flood that ended the MSC. Further recognition of the imprint of the Mediterranean reflooding will lead to fundamental insights into the nature of environmental upheavals, in particular large outburst floods and associated re-establishment of gateways between basins.

GEOLOGICAL SETTING

The study area is situated in the Sicilian Maghrebides, an east–west trending, arcuate, fold-and-thrust belt, linking the African Maghrebides to the Calabrian arc and the Apennines (Butler *et al.*, 1995, 2015; Catalano *et al.*, 1996; Lickorish *et al.*, 1999). This broader area is characterized by a tectonic history of continued accretion of thrust sheets and clockwise rotation of allochthons, since the latest Oligocene (Catalano *et al.*, 1996, 2013). One of the main thrust sheets is the Gela Nappe carrying the wedge-top Caltanissetta Basin as the main depocentre between smaller wedge-top basins in the north (Belice Basin, Ciminna Basin) and the Gela Foredeep and Hyblean

Foreland in the south (Fig. 2). According to palaeomagnetic analysis, the Caltanissetta Basin experienced a *ca* 30° post-Messinian clockwise rotation (Duermeijer & Langereis, 1998).

The Messinian sedimentary successions on Sicily are generally subdivided into various lithostratigraphic units that can be attributed to the three MSC stages described earlier (Figs 1A and 2B). According to Roveri *et al.* (2008b, 2014), Stage 1 is characterized by Primary Lower Gypsum (PLG) deposition in the shallower wedge-top basins, interfingering with marine shales and limestones in the deeper areas (5.97 to 5.59 Ma), Stage 2 is the acme of the MSC and is comprised of Resedimented Lower Gypsum (RLG), halite in the basinal areas and limestones in the marginal areas (5.59 to 5.55 Ma), and Stage 3 is characterized by cyclic alternations of primary evaporites and coarse terrigenous deposits and marls. In the Caltanissetta Basin, the stratigraphic units of Stage 3 consist of the Gessi di Pasquasi Formation (Selli, 1960) or Upper Gypsum (UG) and Arenazzolo Formation (Cita & Colombo, 1979; Manzi *et al.*, 2009). The UG successions generally consist of six couplets of marls and gypsum (cycles 1 to 6) followed by two couplets of marls and sandstones (cycles 6′ to 6″), followed by a final couplet of marls and gypsum (cycle 7) and topped by the Arenazzolo Formation (Fig. 2C). A comprehensive facies and sequence stratigraphic model of the entire UG of the Caltanissetta Basin was established by Manzi *et al.* (2009) and later refined by Andreetto *et al.* (2022a), built on a model that envisages recurring precession-controlled depositional cycles (van der Laan *et al.*, 2006; Hilgen *et al.*, 2007). The stratigraphic position of the Arenazzolo Formation is interpreted inconsistently in literature (see Grothe *et al.*, 2018, for different scenarios). In most cases, the Arenazzolo Formation is depicted as a bounding unit between the UG and the Trubi Formation. Alternatively, it figures as a lateral equivalent of the UG (see figs 2 and 13 in Manzi *et al.*, 2021), although evidence for interfingering between the two units is not observed.

The Arenazzolo Formation is a sandy to silty, locally cross-laminated formation of a few metres thick. It is often genetically linked to a small deltaic system that is also interpreted to have formed the thin sandstone lobes of UG cycles 6′ to 6″ (Schreiber *et al.*, 1976; Roveri *et al.*, 2008a; Manzi *et al.*, 2009). Some have suggested that the Arenazzolo Formation is a distal equivalent of a fanglomerate at the foot of the Peloritan Mountains (Decima & Wezel, 1973), or that it formed in a non-marine littoral setting at the edge of a lake or delta lobe (Cita & Colombo, 1979). Other studies propose that the Arenazzolo Formation is a transgressive sequence implying a significant pre-Zanclean deepening of the Mediterranean (Brolsma, 1978; Londeix *et al.*, 2007; Bache *et al.*, 2012; Popescu *et al.*, 2021). Brolsma (1978) interpreted the Arenazzolo Formation as an initial phase of Trubi deposition rather than a terminal phase of the Messinian evaporation cycles, suggesting a gradual environmental transition between the Arenazzolo Formation and the Trubi Formation. Popescu *et al.* (2009) and Bache *et al.* (2012) consider the Arenazzolo Formation as the expression of an earlier (5.46 Ma) Mediterranean reflooding by Atlantic waters, following a prolonged period of non-deposition represented by the Messinian Erosional Surface (MES) at the base of the Arenazzolo Formation. Their interpretation requires 6.5 precessional cycles and implies that the UG is a lateral equivalent of the fully marine MSC Stage 1. This diverse range of interpretations illustrates the need for a more focused sedimentological study of the Arenazzolo Formation to elucidate its depositional environment.

METHODS

Fieldwork

A total of five sections were analysed (Fig. 3A to C). Sections ERA, ERB and ERC cover the interval between the top of UG cycle 7 and the Trubi Formation, and are exposed along the strip of beach at Eraclea Minoa (37°23′24.18″N, 13°16′36.09″E, Fig. 3B). Section ER6 is located directly north of Eraclea Minoa and comprises UG cycle 6″. Section CR covers part of the Arenazzolo Formation and the boundary with the Trubi Formation at Capo Rosello (37°17′35.40″N, 13°28′10.88″E, Fig. 3A), which is also located along a strip of beach 20 km to the south-east of Eraclea Minoa. Section CR has been studied extensively before (Brolsma, 1978; Cita & Colombo, 1979), but the main part of the Arenazzolo Formation is now covered by a recent landslide. All sections were logged at a 1 cm resolution. Several distinct facies and facies associations were recognized and categorized in all five sedimentary logs (summarized in Tables 1 and 2).

Grain-size analysis

Grain-size analysis was performed on 77 samples in log ERA (11 samples were taken in the

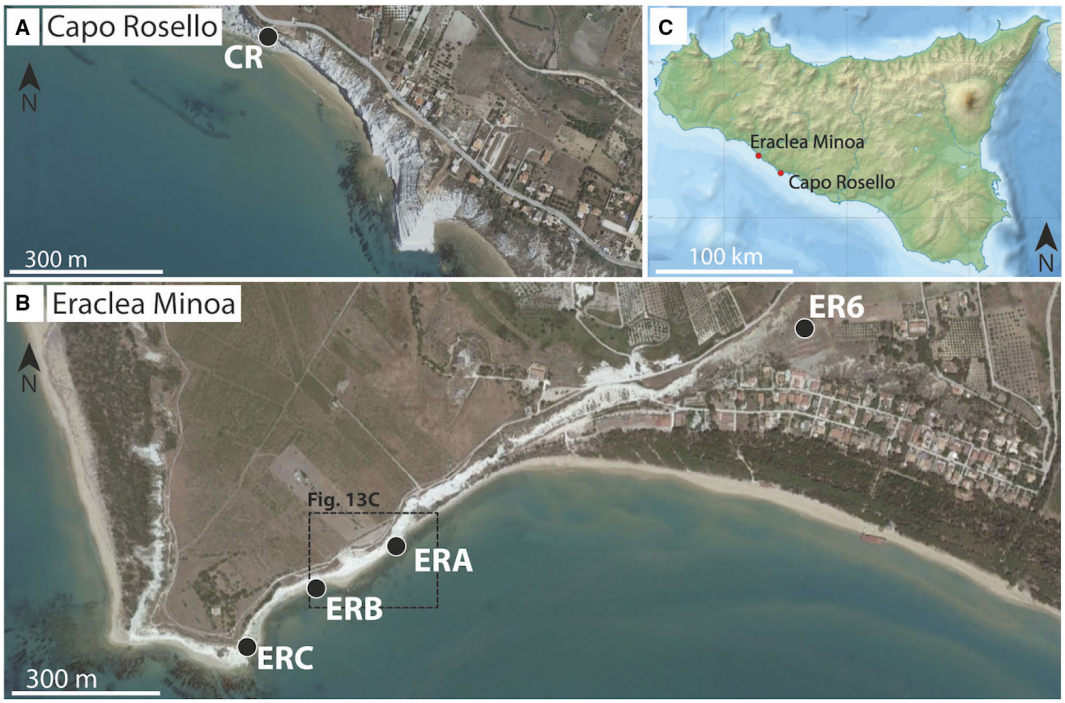

Fig. 3. (A) and (B) Google Earth images of the study areas in Eraclea Minoa and Capo Rosello, including selected locations for sedimentary logging (CR, Capo Rosello; ER, Eraclea Minoa). (C) Location of the two sections on Sicily.

mudstones and sandstones below the Arenazzolo Formation, 64 samples in the Arenazzolo Formation). The aim of this analysis was to: (i) test the facies distinctions made in the field and improve characterization of depositional processes of these facies; and (ii) to generate a record of variation in grain-size distribution throughout the Arenazzolo Formation. The measurements were performed by a Mastersizer 2000 laser particle sizer (Malvern Panalytical, Malvern, UK; for complete methods see Supplementary material S1). Grain size was recorded between 0.2 μm and 2000 μm, subdivided into 100 class intervals. Both sample and subsample duplication were performed and no significant difference in results was found. Grain-size distribution curves and cumulative distribution curves were plotted using Gradistat (Blott & Pye, 2001). Derivation of grain-size parameters was done based on Krumbein & Pettijohn (1938). Calculation of statistical parameters and their physical description is based on the Folk & Ward (1957) graphical method.

Petrographic analysis

A total of 22 thin sections were prepared, covering most of the representative facies. Petrographic analysis was aimed at making qualitative observations of composition, texture and sedimentary structures. Thin sections were scanned using a Leica M165C stereomicroscope (Leica, Wetzlar, Germany). All thin sections were studied in both plane polarized and cross-polarized light using a Leica DM750 optical microscope, and several representative photographs were made, using a Bertrand lens and camera.

Palaeocurrent analysis

Palaeocurrent analysis was performed on trough cross-laminated sandstones of the Arenazzolo Formation at sections ERB and ERA, using an approach based on theory outlined in Slingerland & Williams (1979) and DeCelles *et al.* (1983). High resolution photographs of several two-dimensional exposures of trough cross-lamination were made in the field. The orientation (strike-dip) of the exposures was measured with a geological compass. All laminae sets were interpreted and assigned an estimated trough axis orientation representing the palaeocurrent direction. The procedure of estimating the orientation of the trough axes is explained in more detail in Supplementary material S2.

Table 1. Overview of observed facies. See main text for details.

Formation	Facies	(Short) general description	Bed thickness	Petrographic characteristics (thin section)	Grain-size distribution
Arenazzolo	F11	Brownish to beige very fine sand, decimetre scale convolute lamination.	5–60 cm	–	–
Arenazzolo	F10	Light beige very fine sand, massive bedding. Minor bioturbation	10–50 cm	Compositionally similar to F8 and F9. Massive structureless bedding	Unimodal
Arenazzolo	F9	Beige to grey very fine sand, trough cross-laminated	20–60 cm	Cross-laminated, poorly-sorted. Lithic grains, quartz and bioclasts (mainly foraminifera). Small scale soft sediment deformation	Bimodal, with a fine platykurtic/ mesokurtic peak and coarse leptokurtic peak
Arenazzolo	F8	Beige to grey very fine sand, planar laminated, and organized in centimetre thick cycles, grading in colour from beige to grey (see Fig. 8A). Parting lineation	5–30 cm	Laminated, alternately matrix or clast-supported, poorly-sorted. Lithic grains, quartz and bioclasts (mainly foraminifera)	Bimodal, with a fine platykurtic/ mesokurtic peak and coarse leptokurtic peak
Upper Gypsum	F7	Speckled bed, composed of diatomaceous elongated aggregates	0.3–1 cm	–	–
Upper Gypsum	F6	Mudstone with abundant bivalve shells (shell bed)	3–4 cm	–	–
Upper Gypsum	F5b	Mudstone interbedded with 1–3 mm thick gypsarenites or gypsirudites	5–10 cm	–	–
Upper Gypsum	F5a	Gypsarenite or gypsirudite. Grain size around 2 mm	1–2 cm	Alternately matrix or clast-supported. Poorly-sorted. Composed solely of gypsum clasts with swallow-tail crystal habit, with a mud matrix	–
Upper Gypsum	F4	Lithic or gypsarenite composed of quartz grains and lithic grains with normal grading and sharp undulatory base. Cross-lamination, wavy lamination, and orange to brownish stain at base	1–10 cm	–	–
Upper Gypsum	F3	Mudstones: laminated, bioturbated, sometimes including shell fragments	Highly variable	–	Unimodal

Table 1. (continued)

Formation	Facies	(Short) general description	Bed thickness	Petrographic characteristics (thin section)	Grain-size distribution
Upper Gypsum	F2	Massive orange to greyish bioturbated siltstone	10–40 cm	–	–
Upper Gypsum	F1	Lithic arenite, normal graded, sharp-based. Commonly with erosional bases and with cross-lamination	10–100 cm	Poorly-sorted, matrix-supported, contains monocrystalline quartz, a variety of lithic clasts, and a variety of bioclasts	Bimodal, with a fine platykurtic peak and coarse leptokurtic peak

Table 2. Overview of Facies Associations and their interpreted depositional environments. Further explanation is given in the text.

Formation	Facies Association (FA)	Facies	Depositional environment/processes
Arenazzolo	FA5	Facies 3	Waning of the current depositing FA3 and FA4
Arenazzolo	FA4	Facies 10, Facies 11	Strong intermittent but persistent along-slope bottom current, interrupted by slope failure, in a relatively distal marine setting
Arenazzolo	FA3	Facies 8, Facies 9	Strong intermittent but persistent along-slope bottom current, in a relatively distal marine setting
Upper Gypsum	FA2	Facies 1, Facies 3, Facies 4, Facies 5a, Facies 5b, Facies 6, Facies 7	Relatively distal fluvio-deltaic depositional system
Upper Gypsum	FA1	Facies 1, Facies 2, Facies 3	Relatively proximal, prograding fluvio-deltaic depositional system

RESULTS

Description of sections and outcrops

Log ER6 covers *ca* 7 m of UG cycle 6″ and consists of interbedded sandstones, siltstones and mudstones (Fig. 4). Log ERA covers *ca* 3 m of UG cycle 7, followed by *ca* 7 m of the Arenazzolo Formation. On top of the Arenazzolo Formation a *ca* 50 cm thick clay interval is present and in turn overlain by the Zanclean Trubi Formation (Fig. 5). Log ERB is located 269.5 m to the west of ERA and bears a similar succession, with comparable thicknesses of lithostratigraphic units. ERC is located 142.5 m to the west of ERB and bears the same stratigraphic interval as ERA and ERB but with reduced thickness and without a mud interval right below the Trubi Formation. Between ERB and ERC, an asymmetrical fold pair developed in the interbedded muds and selenitic gypsums of UG cycle 7 (Fig. 5A). This fold has a fold hinge with a trend of 314.8 and a plunge of 10 S. The axial plane is 160.1/22.3 W (Fig. 5B). Log CR only covers the uppermost part of the Arenazzolo Formation, followed by the characteristic top clay layer and the Zanclean Trubi Formation (Fig. 6).

Facies

Eleven facies (F1 to F11, see Figs 7 and 8 for field photographs and Figs 9 and 10 for thin section images) were recognized in the studied sections, and summarized in Table 1.

Facies F1 consists of light beige unconsolidated lithic to bioclastic arenite occurring in single beds

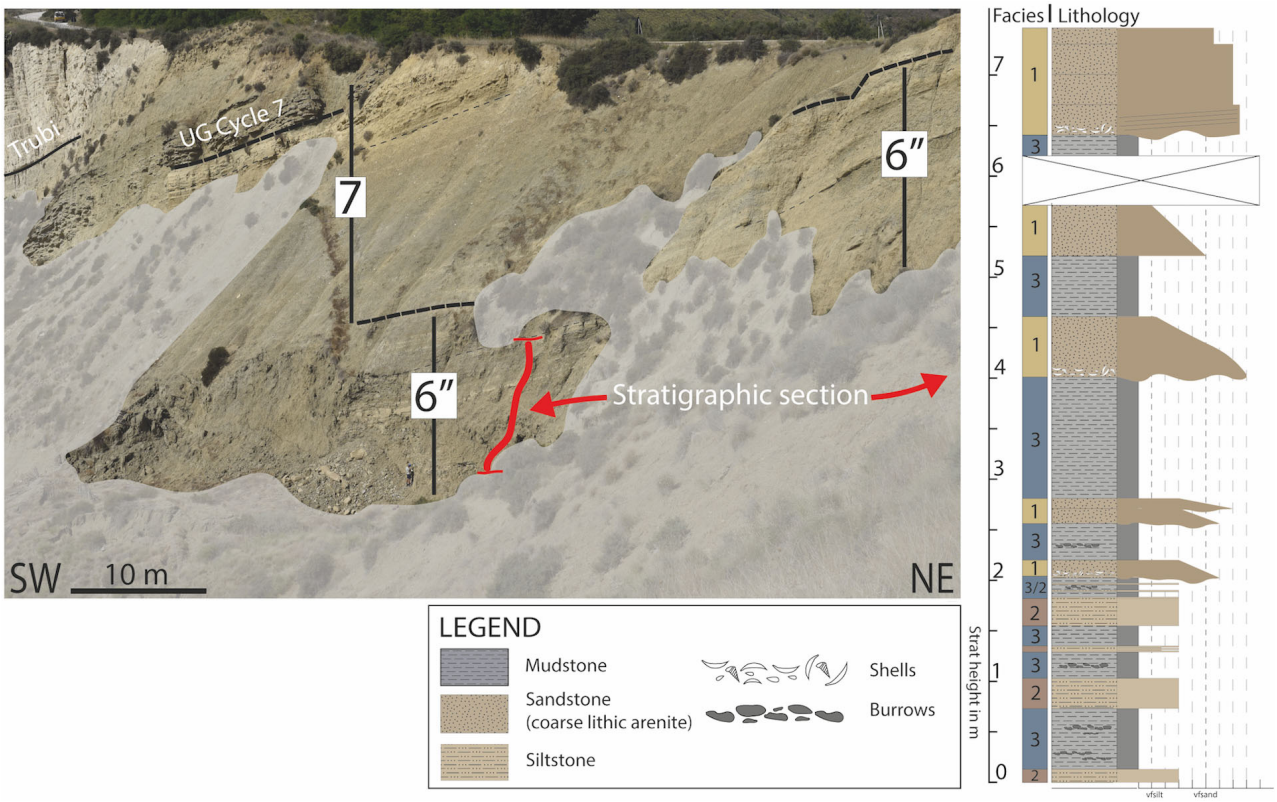

Fig. 4. Sedimentary log and field photograph of section ER6. ER6 is located within Upper Gypsum cycle 6″ (see Figs 2 and 3), below Upper Gypsum cycle 7. The red line indicates the location of the stratigraphic section.

ranging in thickness between 10 cm and 100 cm (Fig. 7A to C). Beds have normal grading and sharp erosive bases and often decimetre-scale to metre-scale low-angle cross-stratification. Petrographically, F1 is dominated by moderately rounded quartz, lithic clasts (including carbonate extraclasts and glauconite), mixed with a heterogeneous assemblage of bioclasts (bryozoans, echinoids and foraminifera) that are relatively large (some are up to 0.16 cm) and fragmented (Fig. 9A to D). Larger bioclasts are concentrated at the bases of beds. F1 is matrix-supported and clear variation in composition and grain size across laminae is rare. In terms of grain-size distribution, F1 is bimodal, very poorly sorted and with a very fine to fine skew (Fig. 7M). F1 has a platykurtic peak between 1 μm and 7 μm (clay to very fine silt) and a major leptokurtic peak between 80 μm and 200 μm (fine sand).

Facies F2 consists of massive orange to greyish bioturbated siltstones, with bed thickness ranging between 10 cm and 40 cm (Fig. 7D). Facies F3 consists of dark greyish mudstone which commonly varies in degree of darkness and intensity of bioturbation (Fig. 7E). Some intervals have mottled, bioturbated portions and are relatively light grey in colour. Other intervals are darker and show no evidence of bioturbation. F3 often bears subtle lamination due to the alternation of relatively muddy intervals and siltier intervals. In some places, broken shell fragments are found floating within the mud, occasionally concentrated in single laminae that have a sharp lower contact and normal grading. In terms of grain size, F3 has a mesokurtic, unimodal, poorly sorted grain-size distribution with a symmetrical skew, and a mean grain size ranging between 3.7 μm and 9.0 μm (very fine silt; Fig. 7N).

Facies F4 consists of lithic arenite to gypsarenite. The framework of this facies is composed predominantly of quartz grains and reworked immature gypsum clasts. Single beds are normally graded and 1 to 10 cm in thickness. They have a sharp undulatory base, often conformable with underlying strata and characterized in some places by flute marks (Fig. 7F to H). Locally,

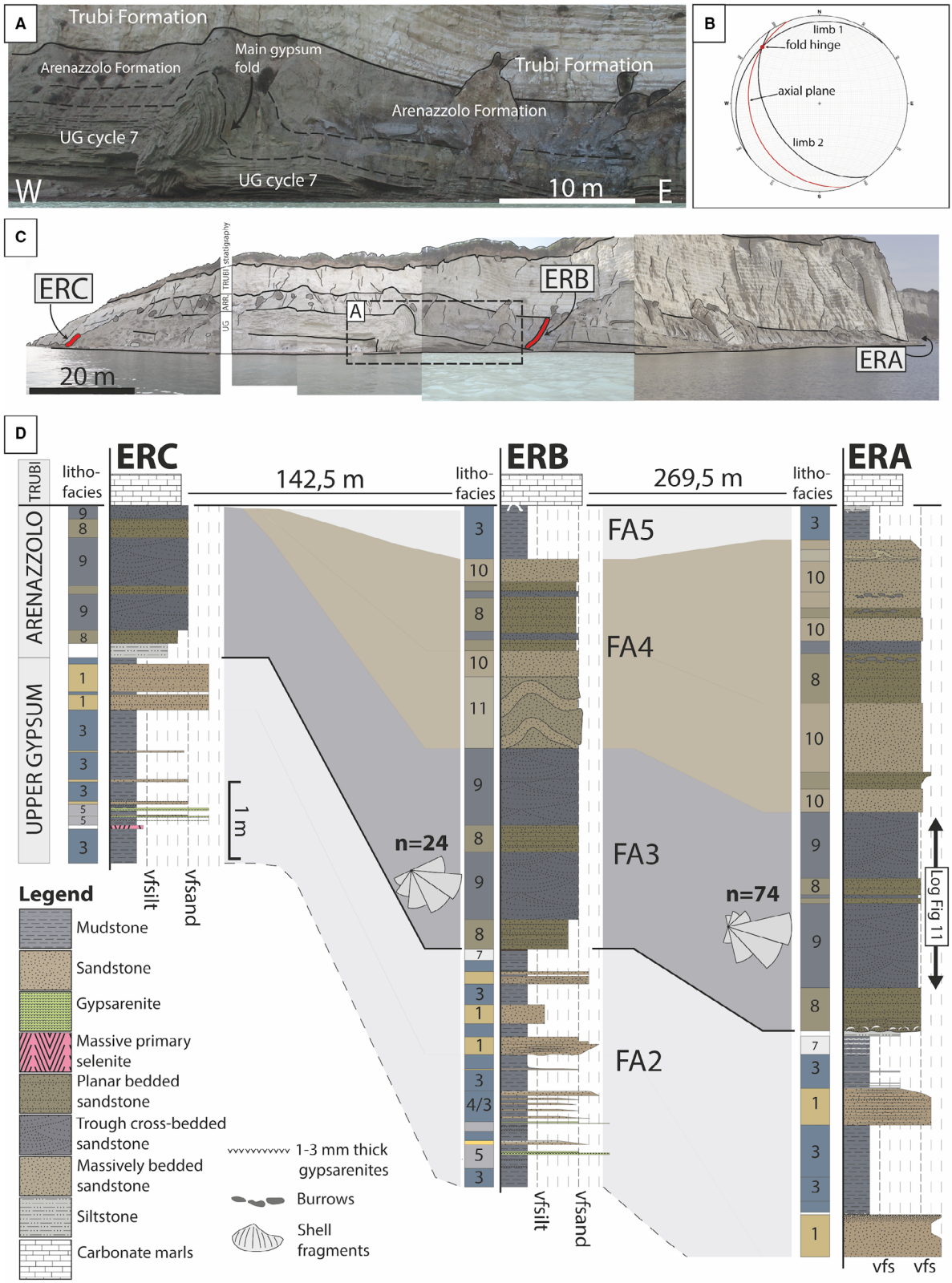

Fig. 5. (A) Selected photograph showing deformation of Upper Gypsum cycle 7, and lateral change in thickness of overlying Arenazzolo Formation (UG, Upper Gypsum; Arr, Arrenazzolo Formation). (B) Fold hinge and axial plane of the folded gypsum. (C) Location of the different logs along the beach south-west of Eraclea Minoa. (D) Sedimentary logs of ERA, ERB and ERC. Stratigraphic position of palaeocurrent measurements are included.

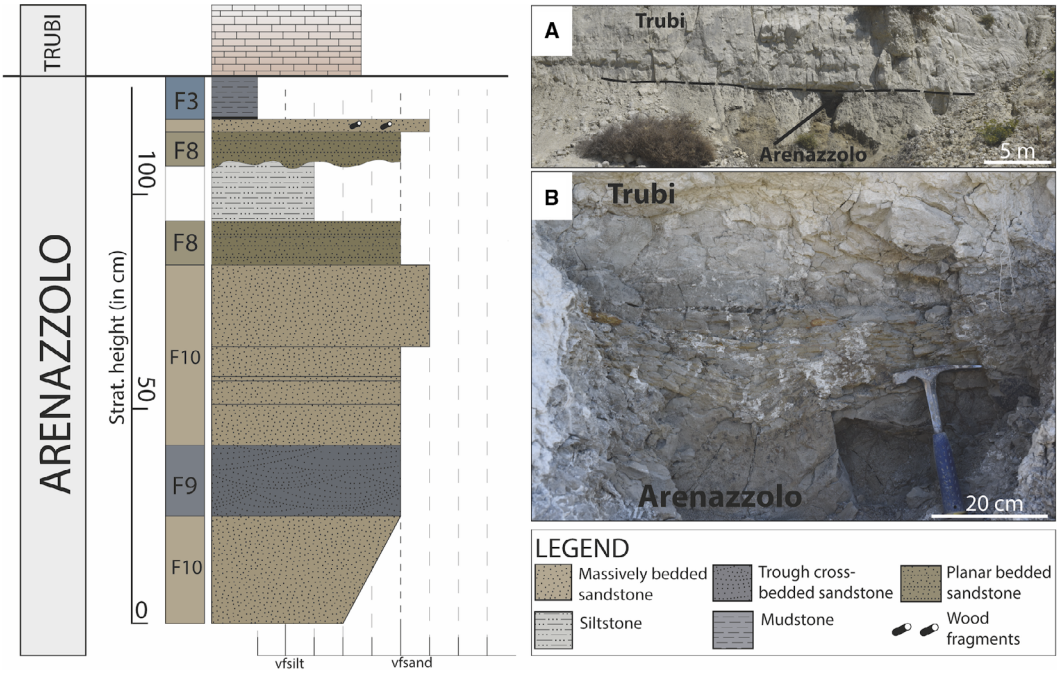

Fig. 6. Stratigraphic log of section CR, covering the uppermost Arenazzolo Formation and Arenazzolo/Trubi (= Messinian/Zanclean) boundary. (A) Logged section. (B) Close-up of the boundary interval.

cross-lamination and wavy lamination is observed, and the bases of single beds often have a brownish to orange stain. In some places, layering is offset by small reverse faulting (Fig. 7G).

Facies F5a is a gypsarenite or gypsirudite. Space between grains is filled by matrix and a whitish cement and clasts are exclusively gypsum in the form of predominantly sand-sized grains. Beds are typically 1 to 2 cm in thickness (Fig. 7I). F5b consists of gypsarenites similar to F5a, but thinner (typically 1 to 3 mm), and interbedded with mudstone. F5b is usually 5 to 10 cm thick (Fig. 7J). Gypsarenites or gypsirudites of F5a and F5b have a framework that is entirely dominated by grains with characteristic swallow-tail crystal habit, evident from thin section images (Fig. 9E and F). In thin section, this facies shows a clear fining-upward trend from grains that are roughly 0.15 cm in diameter to grains that are 0.03 cm in diameter. Texture can be both clast-supported as well as matrix-supported with a matrix that is a beige brownish very fine silt or mud.

Facies F6 is a rudstone (consisting solely of bivalve shells) with a muddy matrix (Fig. 7K). Shells are dominantly intact, and sometimes valves are still connected. In between dominantly intact shells smaller broken fragments occur. Single beds of F6 are between 3 cm and 4 cm thick and usually underlie mudstone intervals that contain minor bivalve shell debris. This facies corresponds to the 'lumachella' horizons, rich in *Dreissena* sp. and *Melanopsis* sp. (Decima & Wezel, 1973; Manzi *et al.*, 2009).

Facies F7 is composed of thin (0.3 to 1.0 cm) layers of detrital elongated diatomaceous aggregates distributed and closely packed in a mud matrix, with both a sharp upper and lower contact (Fig. 7L). These layers have been termed speckled beds by Chang & Grimm (1999). F7 typically interbeds in regular intervals with relatively dark mudstones.

Facies F8 consists of a very fine planar laminated sand, organized in centimetre-thick laminae, grading in colour from beige to grey (Fig. 8A and B). Single beds are between 5 cm and 30 cm in thickness. Colour variations within beds reflect subtle variation in grain size. Although bedding planes are not exposed properly, some fallen blocks in the vicinity of the outcrop show parting lineation (Fig. 8C). Spacing between individual ridges of this lineation is in the order of 1 to 2 cm. The grain-size distribution of F8 is generally bimodal, with very fine to fine skew and a platykurtic to mesokurtic first peak and a second leptokurtic peak. The first peak is at 10 μm and the second peak is between 40 μm and 70 μm

(Fig. 8F). Petrographically, F8 has a relatively uniform composition (Fig. 10A and B). The siliciclastic fraction contains predominantly monocrystalline quartz, black lithic grains (mostly carbonate mudstone intraclasts), and elongated phyllosilicate grains. Besides a siliciclastic fraction, there is a bioclastic fraction that is dominantly composed of small (around 0.25 mm) foraminifera, usually relatively intact, in contrast to the more diverse and coarser bioclast assemblage of sandstones of F1. On the scale of polished thin sections, F8 is clearly laminated and shows compositional and textural differentiation across laminae. Texture varies across laminae between clast-supported, quartz-dominated towards more matrix-supported, composed of phyllosilicates, foraminifera, and a very fine matrix. Both planar lamination as well as low angle downlapping cross-lamination are observed in thin section. Where cross-lamination is observed, the topsets of laminae are well-preserved, and bottom sets show curved downlapping onto underlying erosional surfaces (Fig. 10A and B). In some places, laminae have undergone soft sediment deformation, and show flame structures that are oriented in the same direction as the dip of laminae foresets (Fig. 10A). Intervals with soft sediment deformation are truncated at the top by erosional surfaces.

Facies F9 is a beige to grey very fine trough cross-laminated sand (Fig. 8D). Single beds are between 20 cm and 60 cm. Wavelength of single troughs is between 8 cm and 22 cm, and amplitude of troughs is typically between 2 cm and 4 cm. Variation in trough dimensions occurs throughout the interval and troughs are usually higher in wavelength and lower in amplitude close to intervals of planar laminated sandstones of F8 (Fig. 11). Laminae are mostly angular but become slightly tangential or sigmoidal when the face of exposure is parallel to the trough axis. Grain-size variation is reflected in colour variations across laminae sets. In terms of grain-size distribution and petrography, this facies is similar to F8 (Fig. 10C).

Intervals composed of F8 and F9 show a distinctive vertical grain-size trend throughout sections, coincident with variations in bedform dimensions. For the interval between 300 cm and 600 cm stratigraphic height in ERA, this variation is plotted in Fig. 11A. Generally, planar laminated sandstones (F8) are characterized by coarser grain size than trough cross-laminated sandstones (F9). Between 380 cm and 470 cm, a clear coarsening-upward sequence is observed, where grain size increases gradually from roughly 10 μm to roughly 35 μm. This coarsening sequence is coeval with a gradual change from high amplitude, low wavelength troughs, to low amplitude, high wavelength troughs, and finally to planar laminae (as illustrated in the interpreted photograph, Fig. 11B).

Facies F10 is a light beige very fine sand with massive bedding (Fig. 8E). F10 shows minor bioturbation in some intervals. Bed thickness is typically between 10 cm and 50 cm. Grain-size distribution of F10 is unimodal, poorly sorted and has a symmetrical to fine skew. Mean grain size ranges between 12 μm and 18 μm (medium to coarse silt). Petrographically, F10 is different and stands out from the other Arenazzolo Formation facies because it lacks evident traction structures (Fig. 10D).

Facies F11 is a brownish to beige very fine sandstone with decimetre-scale convolute lamination that is truncated by overlying massively bedded sandstones of F10 (Fig. 8E). Bed thickness varies between 5 cm and 60 cm. Colour variation between blue and beige/brown across laminae and different intervals is similar to the colour variation observed in F8 and F9.

Facies interpretations

F1 was formed by rapid deposition from gravity-driven density currents, evident from their structureless and poorly sorted texture on micro-scale, and normal grading and sharp base on bed scale. Compositional heterogeneity indicates a relatively proximal sediment source. The absence of erosional structures within single beds is evidence that beds resulted from single phases of deposition. Variations in thickness and grain size among F1 beds probably reflect different degrees of distality with respect to the source area. F2 was also formed by gravity-driven density currents decelerating and depositing silt, probably as a (distal) equivalent of F1. F3 was formed by background settling and periodic burrowing in a relatively quiet environment. The dark colour of this facies is indicative of the periodic development of oxygen-poor conditions. F4 was formed by density currents with a relatively large contribution of immature gypsum fragments, indicating the proximity of a gypsum source. The undulatory base, wavy lamination and small-scale reverse faulting of many of these layers relates to syn-sedimentary or post-sedimentary deformation after rapid

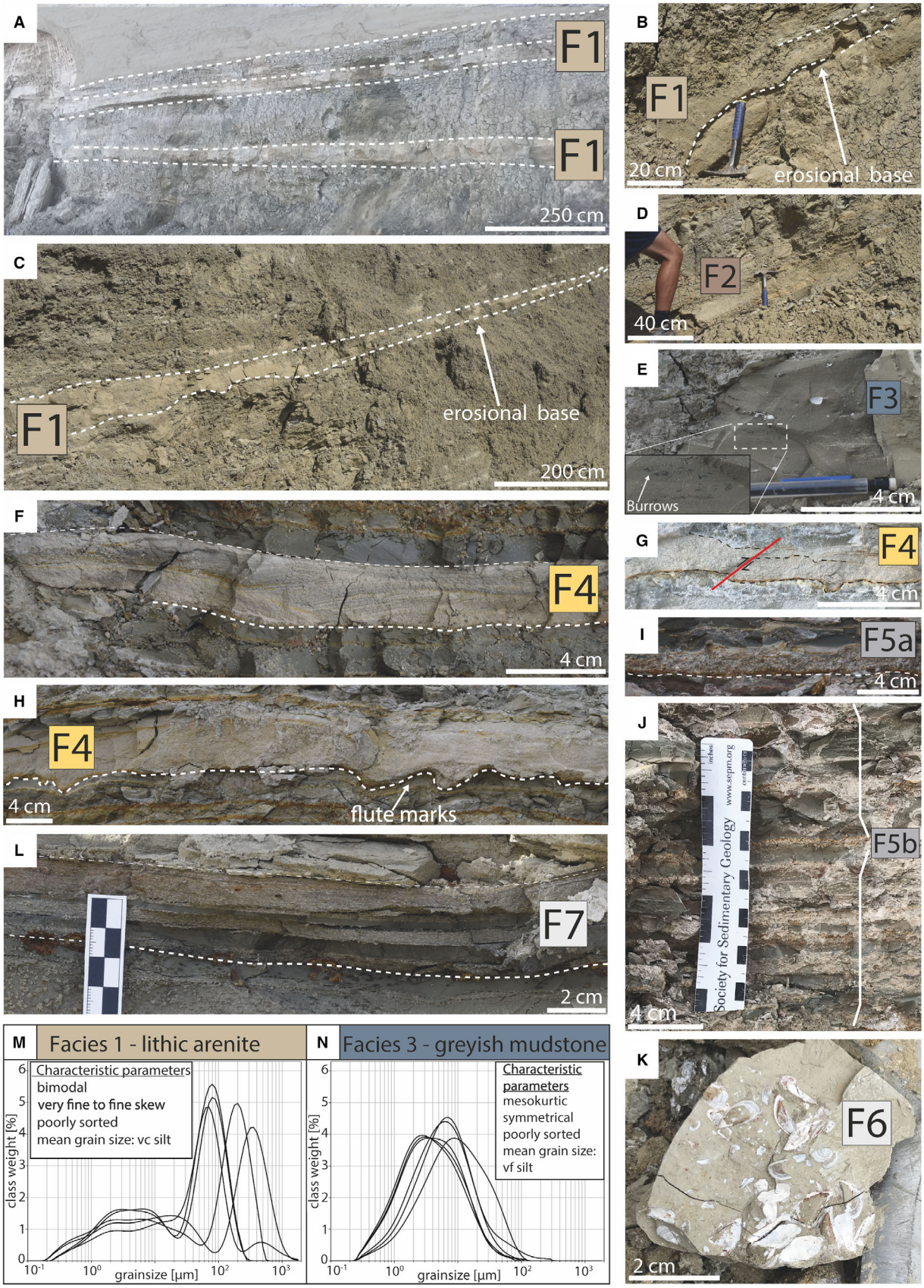

Fig. 7. Selected photographs of F1 to F7. (A) Two subsequent beds of thick lithic arenites (F1). (B) Lithic arenite with erosional base (F1). (C) Lithic arenite with erosional base (F1). (D) Siltstone (F2). (E) Burrowed mudstones (F3). (F) Lithic arenite with predominantly gypsum clasts (F4). (G) Lithic arenite with small reverse fault (F4). (H) Lithic arenite with flute marks (F4). (I) Gypsarenite (F5a). (J) Interbedded muds and gypsarenites (F5b). (K) Shell bed (F6). (L) Speckled beds and interbedded mudstones (F7). For F1 (n = 5) and F3 (n = 7) measured grainsize distributions are included (M) and (N).

deposition on top of water saturated muds. Facies 5a and 5b originated from erosion of a nearby gypsum source, and subsequent transport and deposition, without any mixing with grains from other sediment sources prior to deposition. Shell beds of F6 were deposited by the accumulation of bivalve shells and pelagic settling in a well-ventilated water column, which was occasionally colonized by bivalves and other burrowing organisms, in contrast to the more restricted and stagnant water column in which F3 muds were deposited. Deposition of F7 results from the upslope entrainment and downslope transport of diatomite aggregates (Chang & Grimm, 1999).

F8 and F9 were deposited by a fluctuating but overall persistent bottom current, evident from several observations. First of all, F8 and F9 are the result of continued accretion of sand of rather uniform grain size and composition, combined with the continued influence of traction and suspension (expressed in trough cross-lamination and planar lamination). Trough cross-laminated sandstones (F9) represent the relatively weak currents. Planar laminated sandstones (F8), with a slightly higher mean grain size and parting lineation on bedding planes represent the stronger currents, probably in an upper stage plane bed flow regime (hence the parting lineation). The common variation in size and geometry of laminae and cross-sets of the trough cross-laminated sandstones suggest that also within single facies intervals, current speeds were fluctuating. Second, coarsening-upward grain-size trends of several tens of centimetres, coeval with changes in bedforms, are a strong indicator of a gradually increasing current strength (Fig. 11). Third, thin section images of F8 and F9 show compositional and textural difference across laminae that reflect the repeated change between bedload deposition and deposition out of suspension. Local reactivation surfaces illustrate short episodes of erosion, followed by resumption of deposition. The presence of millimetre-scale mud-clasts within a matrix of very fine sand, suggests that currents had erosional capability to erode nearby muddy or silty seabed. In addition, the preservation of topsets in cross-laminated intervals and the presence of soft sediment deformation indicates high sedimentation rates. Besides evidence for fluctuating current action, deposition of F8 and F9 was also relatively distal. The lower variety of lithic clasts observed in thin section, the fine grain sizes and the absence of coarse shallow marine benthic bioclasts suggests that deposition of the Arenazzolo Formation (F8 and F9) was more distal than sandstones of the UG (F1). In addition, the sudden appearance of elongated phyllosilicates implies the influence of an additional source. The fine platykurtic to mesokurtic peak around 10 μm for F8 and F9 could be caused by an additional (metamorphic) source that delivered these phyllosilicates. Finally, the relative absence of the finest grain-size fraction in F8 and F9 could be the result of stronger winnowing action during deposition, which seems plausible in a scenario with strong persistent currents.

F10 formed during rapid instantaneous deposition of sand (while the formation of traction structures was suppressed), in contrast to F8 and F9 that resulted from alternating phases of erosion and deposition creating centimetre-scale traction structures. F11 is characterized by decimetre-scale convolute laminations which typically form right after or during deposition when a sediment bed is in a temporarily weakened state (Kuenen, 1953; Middleton, 2003; Bjørlykke, 2015). Triggers for such lamination to form can be various: water waves, unusually rapid sedimentation, or seismic triggers are the most likely ones (Owen & Moretti, 2011).

Facies Associations

Sedimentary facies are linked to form five distinct Facies Associations (FA) based on regular recurrence of vertically related facies. Facies Association 1 (UG) occurs in section ER6

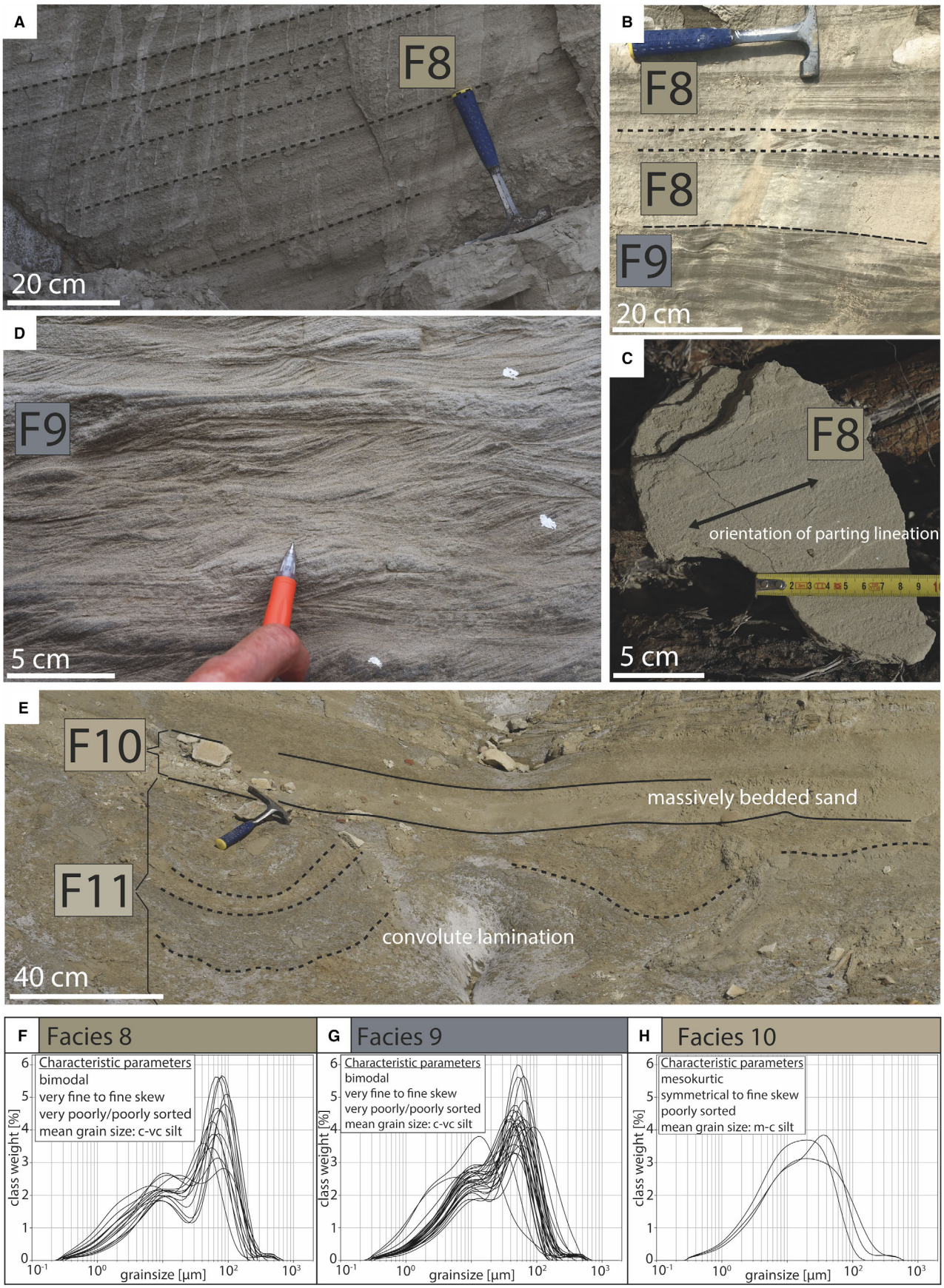

Fig. 8. Selected photographs of F8 to F11. (A) Planar laminated sandstone (F8). (B) Alternation of planar laminated sandstones and trough cross-laminated sandstones (F8 and F9). (C) Trough cross-laminated sandstone (F9). (D) Fallen block showing the bedding plane of a planar laminated sequence (F8) with parting lineation. (E) Beds of convolute laminated sandstone (F11), and massively bedded sandstone (F10). Included are three grain-size distribution graphs of F8, F9 and F10 (F) to (H).

(Fig. 4). The lower part of this FA consists of interbedded silts (F2) and mudstones (F3), transitioning upward into interbedded sandstones with erosional bases (F1) and bioturbated mudstones (F3). Facies Association 2 (UG) is composed of gypsarenites (F5a), interbedded muds and gypsarenites (F5b), sandstones (F4) and mudstones (F3). Upward, FA2 changes to

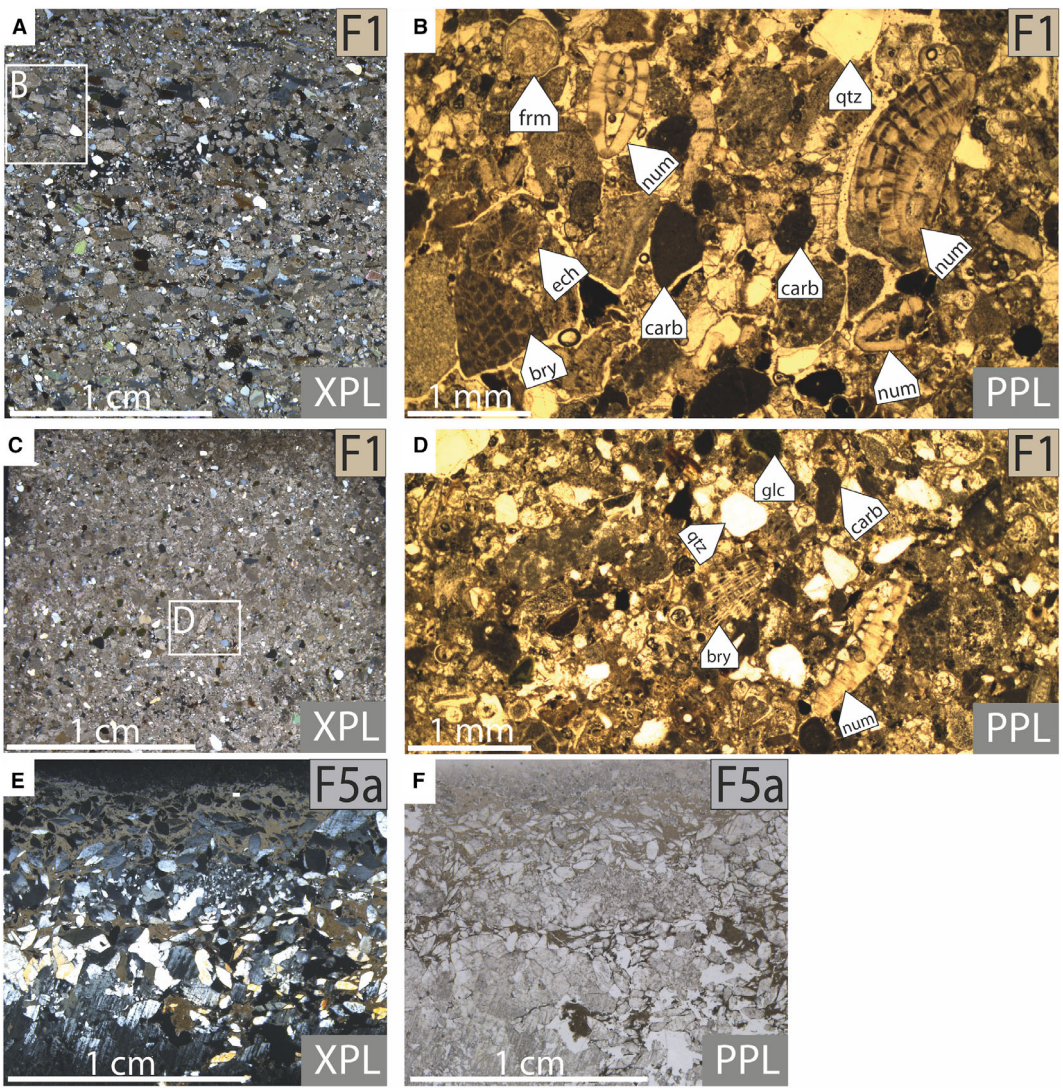

Fig. 9. Scans of polished thin sections and optical micrographs of F1 and F5a (XPL – cross-polarized light and PPL – plane-polarized light). (A) to (D) Matrix-supported lithic arenite (F1) with a framework composed of monocrystalline quartz (qtz), lithic clasts [including carbonate mudstones (carb)], glauconite (glc) and a diverse assemblage of shallow marine bioclasts [including foraminifera (frm), nummulites (num), echinoids (ech) and bryozoans (bry)]. (E) and (F) Gypsarenite (F5a).

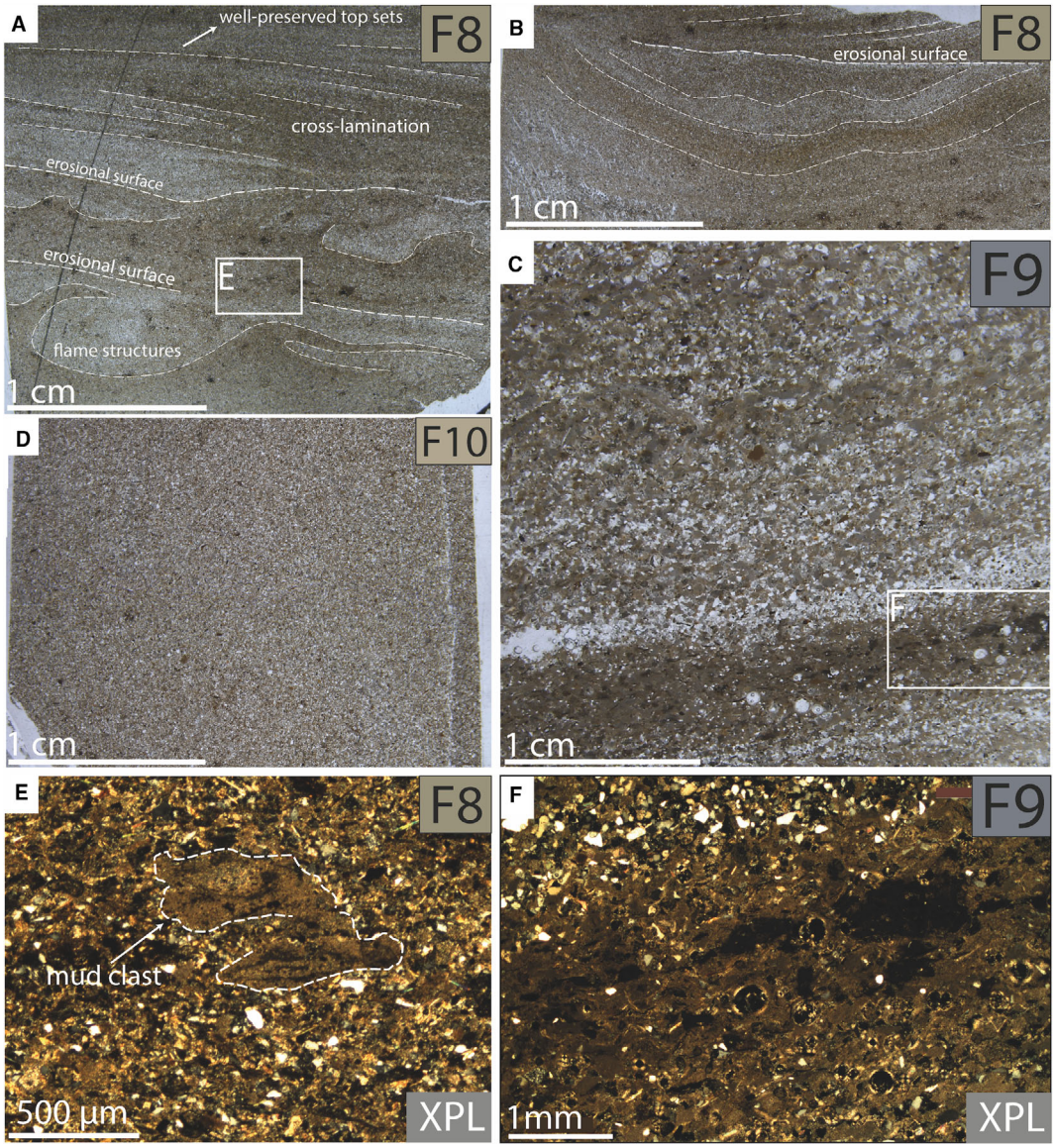

Fig. 10. Scans of polished thin sections and optical micrographs of samples from the Arenazzolo Formation (F8, F9 and F10). (A) Massively bedded, structureless sand (F10). (B) Laminated sand with a distinct interval of concave-up soft sediment deformation, truncated by an erosional surface and overlain by cross-laminae (F8). (C) Laminated sand with two deformed sequences with flame-structures, and one sequence of cross-laminated sand with well-preserved top-sets (F8). The lowermost part of the interval shows mud-clasts of which a close-up is depicted in (E). (D) Relatively coarse laminated sand (F9), showing compositional and textural difference across laminae [close-up in cross-polarized light – XPL – is depicted in (F)].

an interbedding of well-burrowed mudstones (F3) and decimetre-thick sandstones (F1) which are locally topped by shell beds (F6).

Facies Association 3 (Arenazzolo Formation) is composed of alternating planar laminated (F8) and trough cross-laminated (F9) sandstones. Boundaries between facies are generally sharp, although in some intervals more gradual transitions occur between high amplitude trough cross-laminated sandstones and planar laminated sandstones. FA3 is followed by a sequence of massively bedded (F10) and convolute laminated sandstones (F11) comprising FA4 (Fig. 4).

Facies Association 4 is 75 cm thick in both ERA and ERB but thins outs and disappears

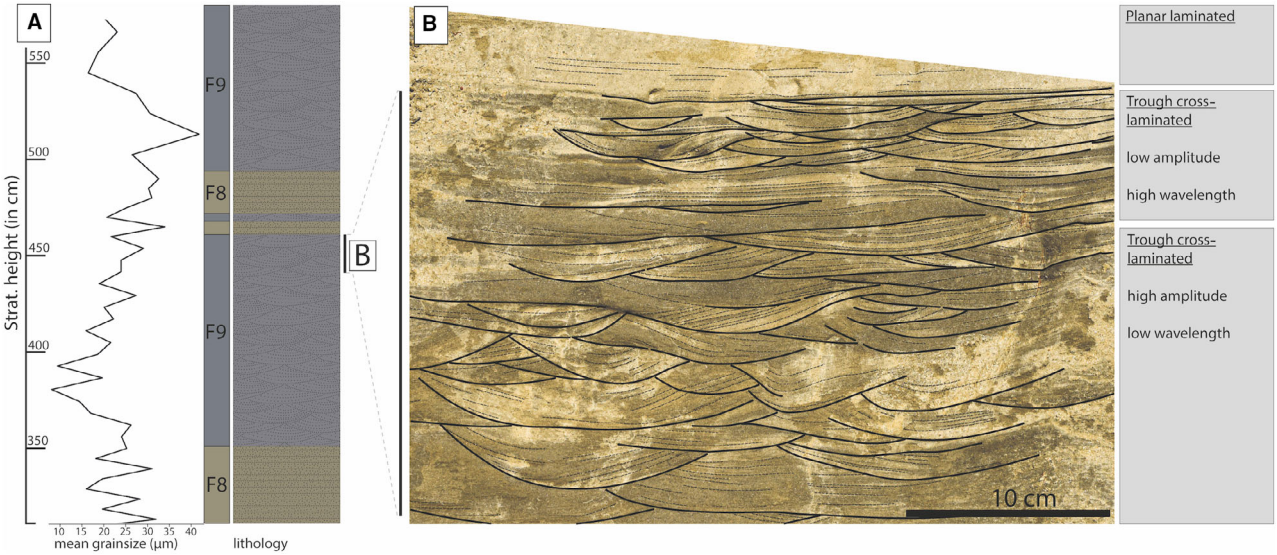

Fig. 11. (A) Grain-size record of the interval between 300 cm and 600 cm in log ERA. Between 380 cm and 470 cm stratigraphic height, a coarsening-upward trend is observed, coeval with a change in bedform dimensions. (B) Close-up of the boundary between cross-laminated and planar laminated sequences at 450 cm stratigraphic height, illustrating a gradual change in bedform dimensions.

towards ERC, west of the asymmetrical fold pair. FA4 is thus syn-kinematic to the deformation of the selenitic gypsum of UG cycle 7.

Facies Association 5 is an interval dominated by mudstones (F3) that change in colour from light grey to dark grey upward in the stratigraphy (Fig. 6). Locally, wood fragments and siltier intervals are found within the mud. The transition between FA5 and the whitish Trubi marls coincides with the Messinian/Zanclean boundary and is characterized by abundant trace fossils. Centimetre-scale burrows penetrate the uppermost clays of FA5 and are filled by whitish marls of the Trubi Formation.

Palaeocurrent directions

The approximate directions of trough axes of interpreted laminae sets in FA3 are presented in Figs 12 and 13, based on two exposures of the lowermost Arenazzolo Formation (see Fig. 5 for the stratigraphic position, and Appendix S1 and S2 for detailed measurement technique). The results of exposure ERA (with a strike orientation of 02°) and exposure ERB (with a strike orientation of 80°) were combined. This yielded a palaeocurrent direction that is east to south-east (Fig. 13), without correction for tectonic rotation.

DISCUSSION

Reconstruction of the palaeoslope

Using the geometry of strata confining the deformation of UG cycle 7, the palaeoslope of the study area can be reconstructed. Deformation of UG cycle 7 is typical for subaqueous gravitational sliding of a layered sequence on an unstable slope, in which sliding is directed perpendicular to the strike of the slope (Strachan & Alsop, 2006). The mechanical stratigraphy of selenite gypsum interbedded in softer marls facilitated the short wavelength folding in the gypsum (see Butler *et al.*, 2015). Field measurements indicate that the fold hinge is directed roughly north-west (strike of 314.8, see Fig. 5). Correcting for the *ca* 30° clockwise post-Messinian rotation of the Caltanissetta Basin (Duermeijer & Langereis, 1998), this means that the Messinian palaeoslope at Eraclea Minoa was dipping towards the north/north-east (Fig. 14A), which is in accordance with earlier structural and palaeogeographical reconstructions of the Messinian Caltanissetta Basin (Lickorish *et al.*, 1999; Manzi *et al.*, 2021). It also implies that the dominant palaeocurrent direction (see Figs 13 and 14) was directed roughly along the regional slope (i.e. towards the east/south-east).

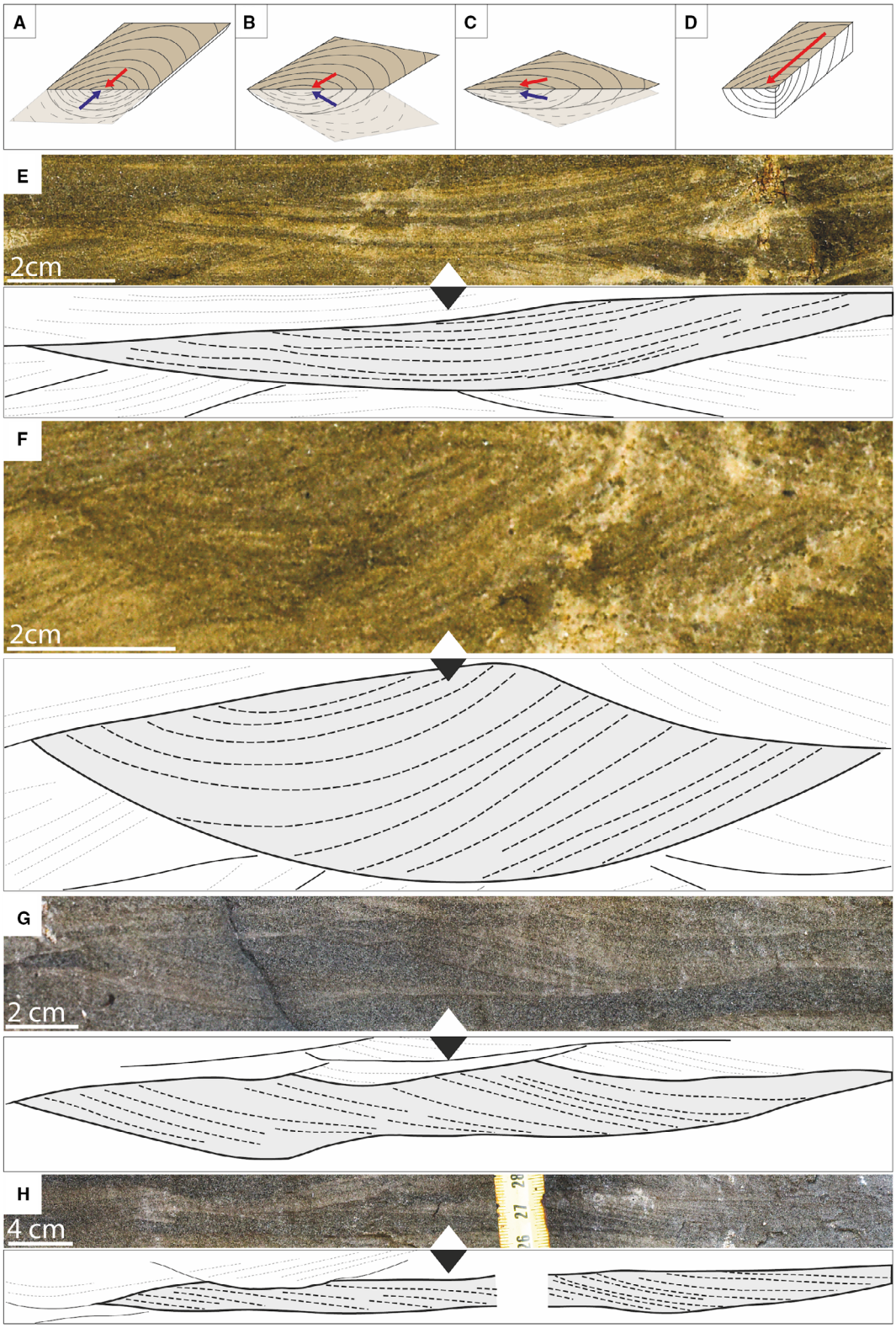

Fig. 12. Various possible trough cross-lamination geometries, in theory (A) to (D) and as observed in the field (E) to (H). Blue and red arrows in (A) to (D) indicate possible trough axis orientations. (A) corresponds to (E), (B) corresponds to (F), (C) corresponds to (G) and (D) corresponds to (H). Note that (D) has only one possible trough axis orientation.

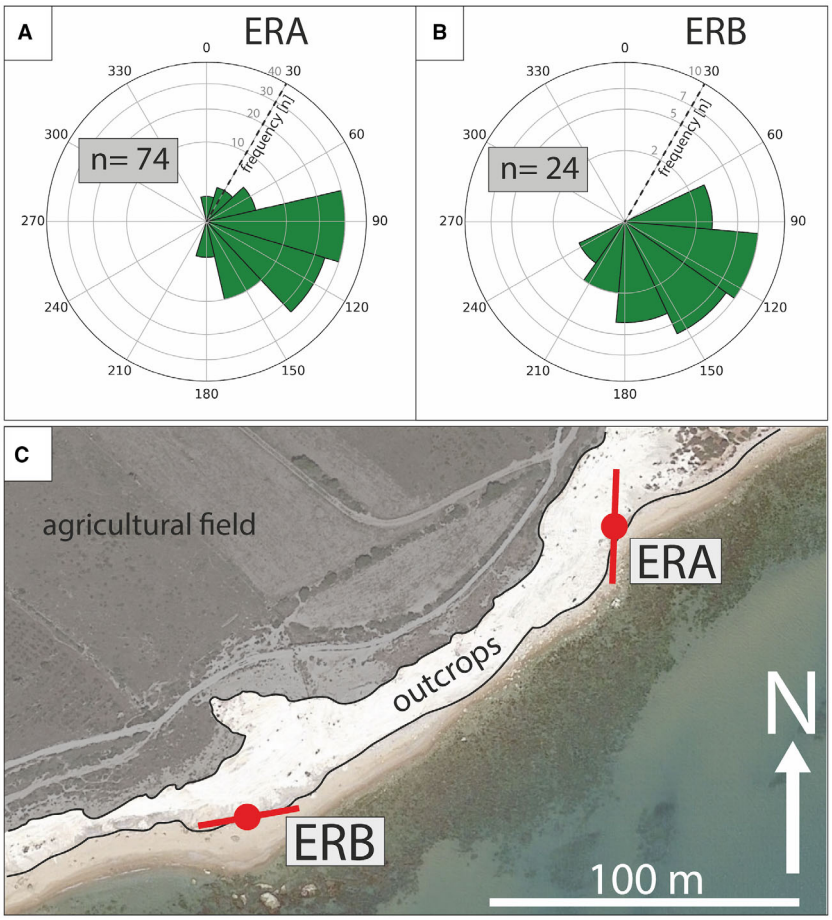

Fig. 13. (A) and (B) Rose diagrams of palaeocurrent measurements at ERA and ERB (see Fig. 5 for stratigraphic position). Width of individual columns corresponds to a bin size of 30°. (C) Location and orientation of exposures (location is indicated with a red dot and orientation of the exposure is indicated with a red line).

Fluvio-deltaic deposition of the upper gypsum (FA1 and FA2)

Sedimentological interpretation

Facies Association 1 records the progradation of a fluvio-deltaic system, characterized by a transition from distal prodeltaic mudstones (F3) and siltstones (F2) deposited by flood-related density currents to deltaic channel sandstones or interdistributary bay sandstones (F1), which were deposited down-slope in a more proximal delta-front environment (Fig. 15A). This interpretation is consistent with earlier work on transport directions of resedimented gypsum in the Caltanissetta Basin (Manzi *et al.*, 2009) and also fits general facies models of fluvio-deltaic systems in tectonically active foreland basin systems (Mutti *et al.*, 2000; Bhattacharya, 2006). Sandstones (F1) in this facies association generally hold a wide assemblage of redeposited shallow heterogeneous marine bioclasts and immature lithic clasts (Fig. 9), indicative for a deltaic system entering a shallow marine/lacustrine environment, eroding and redepositing sediment fed by a nearby source. FA2 was deposited in a similar fluvio-deltaic system as FA1 but with a different source area. The frequent occurrence of redeposited selenites (F4, F5a and F5b) occurring in FA2 and not in FA1, suggests that erosion and redeposition occurred while primary selenites were not significantly buried yet, and could thus be reworked.

Palaeogeographical reconstruction

Fluvio-deltaic deposition of FA1 and FA2 (Fig. 15A) took place in the main Caltanissetta wedge-top basin (Roveri *et al.*, 2008b). Variability in distality of facies was controlled by precessional climatic changes and sediment supply (Manzi *et al.*, 2009; Andreetto *et al.*, 2022a). The degree to which the Caltanissetta Basin was connected to other basins is uncertain. Some studies suggest that at least a partial connection between western and eastern Mediterranean subbasins must have prevailed during UG deposition,

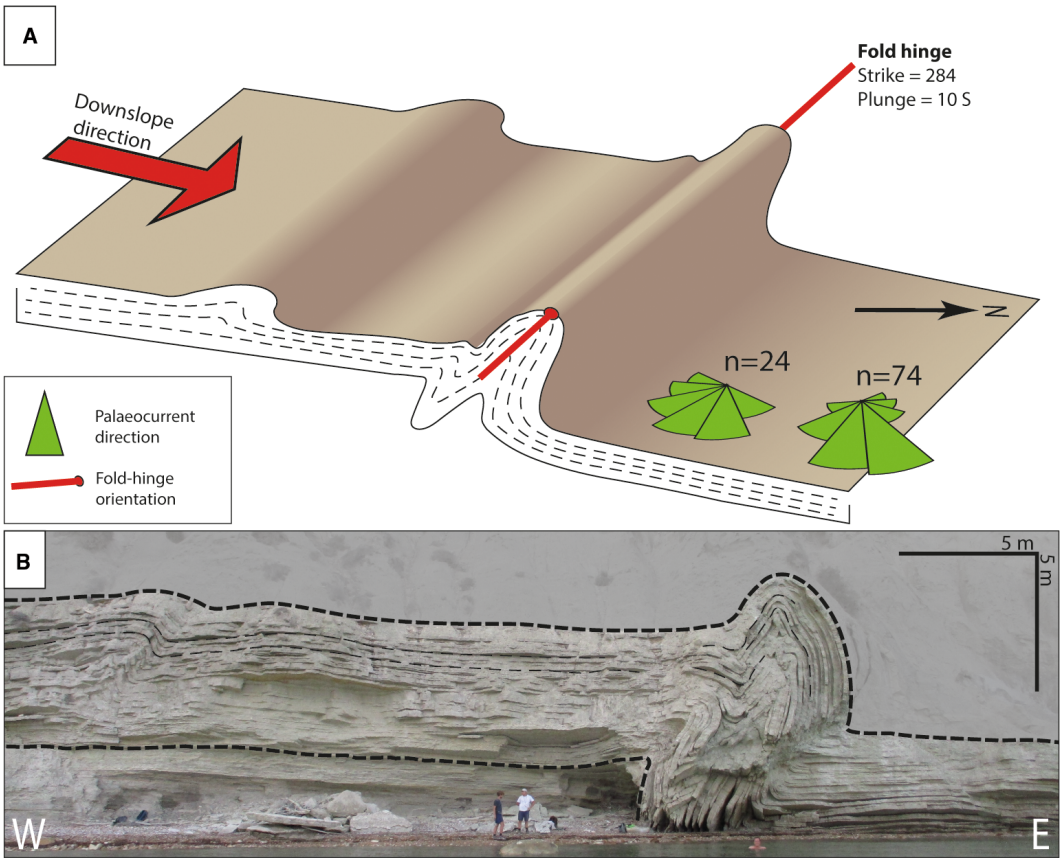

Fig. 14. Reconstruction of the regional slope. (A) Shows the envisioned deformation of Upper Gypsum cycle 7 and the interpreted relationship with the palaeoslope and measured palaeocurrents. The fold hinge has a strike of 284° (after correction for 30° clockwise rotation) which means that the palaeoslope was dipping to the north to north-east. Note that rose diagrams indicate along slope transport direction. (B) Field photograph of the folded Upper Gypsum, used for the palaeoslope reconstruction.

especially during highstands (Andreetto *et al.*, 2021). The main argument for this is that high water-level conditions are necessary to explain the presence of Paratethyan ostracods in marginal Mediterranean subbasins (Gliozzi *et al.*, 2007; Stoica *et al.*, 2016) and their $^{87}Sr/^{86}Sr$ signature, which reflects the mixing between local river water and an anomalohaline water mass filling the open Mediterranean Basin (Andreetto *et al.*, 2021, 2022a, 2022b). In addition, many authors interpret a general transgressive trend throughout the upper part of the UG which could be a precondition for Atlantic floods to periodically cause incursions (Butler *et al.*, 1995). Still, water level must have been able to get low enough to disconnect the basin and oversaturate the brine to such a degree that gypsum could precipitate, favouring a scenario where the water level was, at least periodically, relatively low in the Caltanissetta Basin (as illustrated in Fig. 15A).

The Caltanissetta Basin follows a general proximal to distal trend from north to south, reflected in fractionation of grain size, and distality of facies (Maniscalco *et al.*, 2019), as well as thickness variation of the UG throughout the basin (Manzi *et al.*, 2009). In the current study's analyses, the sandstones of FA1 and FA2, are considered as distal equivalents of coarser UG facies in the north. The thrust nappes bordering the basin in the north are a logical sediment source for these sandstones. In addition, the Gela thrust front, located south from Eraclea Minoa may have provided an additional sediment source, subaerial or submarine (Manzi *et al.*, 2021). This is also supported by the observation that the regional slope was dipping north-eastward during later deposition of the Arenazzolo Formation (see Figs 13 and 14).

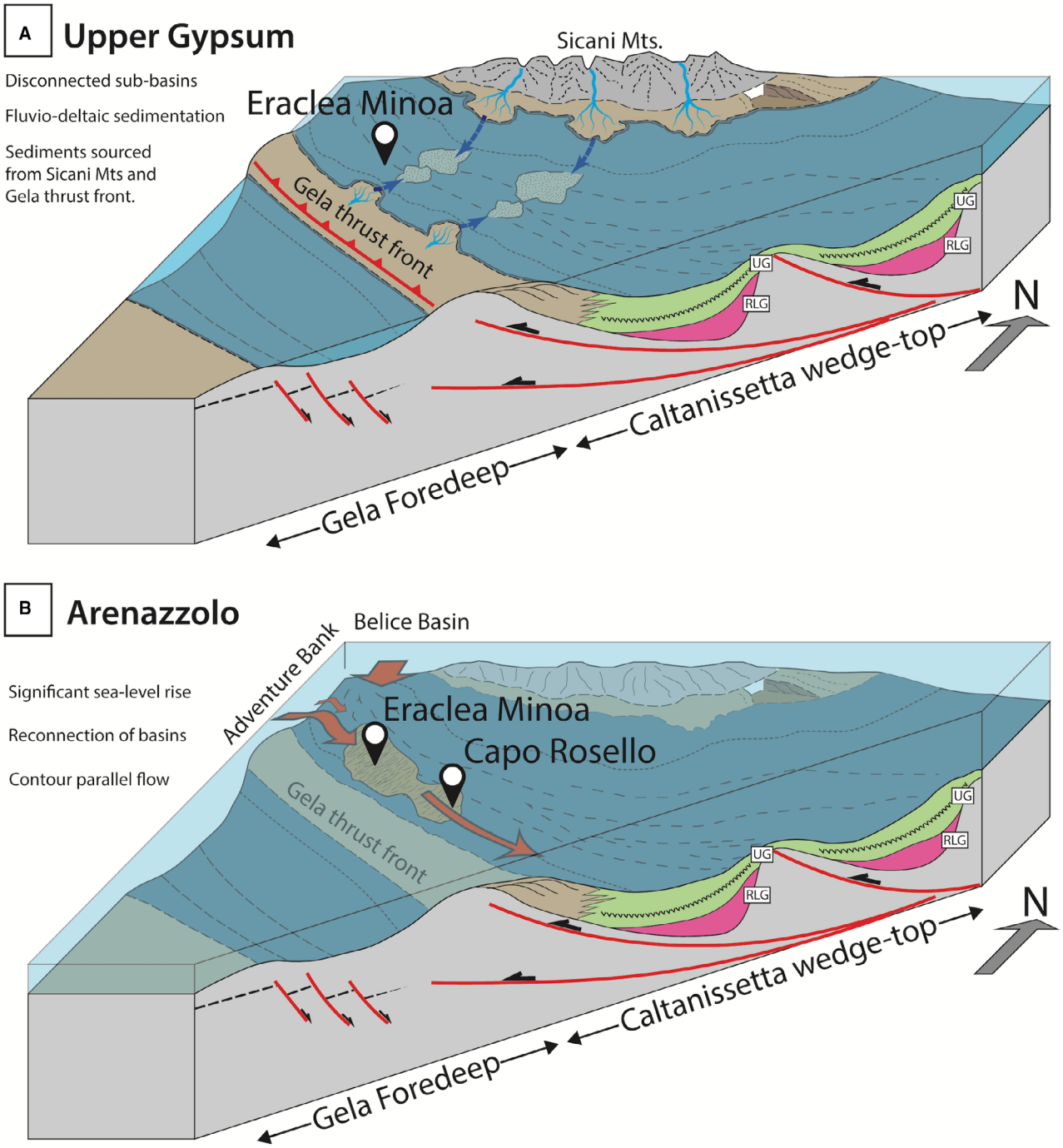

Fig. 15. Schematic palaeogeographical scenarios for deposition of the uppermost Upper Gypsum (UG) sandstones and the Arenazzolo Formation. Palaeogeography is based on tectonic information (Lickorish *et al.*, 1999; Roveri *et al.*, 2008a,b; Catalano *et al.*, 2013; Manzi *et al.*, 2021). (A) Scenario for Upper Gypsum deposition with disconnected sub-basins and proximally sourced sediment from the north and possibly from the Gela thrust front. (B) Arenazzolo Formation scenario after transgression and reconnected western and eastern Mediterranean, with along-slope currents forming a sandy contouritic drift. RLG, Resedimented Lower Gypsum; UG, Upper Gypsum.

Transgression and establishment of a bottom current (FA3, FA4 and FA5)

Sedimentological interpretation

Onset of the contour parallel current of the Arenazzolo Formation (FA3). FA3 represents a clear change in depositional style, compared to underlying UG deposits of FA1 and FA2. FA3 deposition was submarine, given the abundant marine microfauna in the sediment (Londeix *et al.*, 2007). Whereas deposition of FA1 and FA2 was governed by episodic density currents and background settling, deposition of FA3 was governed by strongly fluctuating but persistent along-slope currents. The Arenazzolo Formation is a relatively shallow contouritic deposit that was formed along the local physiography of the Gela thrust front (Fig. 15B).

Key results of the analysis of the Arenazzolo Formation presented here are in line with established facies models of contourites. First of all, traction structures like cross-lamination and planar lamination (as observed in FA3) have been recognized in many contourites (Shanmugam *et al.*, 1993; Mutti & Carminati, 2012), and ripples, lineations and other bedforms have been recognized in modern-day bottom current systems (Stow *et al.*, 2013; Rebesco *et al.*, 2014; Esentia *et al.*, 2018). Continuous accumulation of sand, uninterrupted by phases of sediment starvation, and the relatively hostile late Messinian environments likely prevented bioturbation (which is often used to interpret contourites) from destroying traction structures and explains why they are well-preserved. Second, palaeocurrent reconstruction and slope orientation (Fig. 14) suggest a contour-parallel current direction, which is a crucial diagnostic feature in many contourite studies. Also, the lateral correlation of individual cross-laminated and planar laminated facies over *ca* 400 m (see FA3 in Fig. 5) suggests that these facies are likely part of a larger sandy contourite drift system. In addition, the shift from relatively fine (*ca* 10 μm) to coarser (*ca* 35 μm) grain size, coeval to the change from trough cross-lamination to planar lamination (as documented in ERA, Fig. 11) fits with the interpretation of a contourite (Gonthier *et al.*, 1984). In theory, the contourite model includes a shift from weak to strong currents and a shift back to weak currents, reflected in a bi-gradational sedimentary sequence. In the case of the Arenazzolo Formation, at least, this shift from weak to strong currents is present (Fig. 11).

Slope instability during deposition of the Arenazzolo Formation (FA4). Massively bedded sandstones and decimetre-scale convolute laminated sandstones of FA4 overlie FA3 and are syn-depositional or slightly post-depositional to the deformation of UG cycle 7, evidenced by the western pinch-out of FA4 (see Figs 5 and 14). The formation of FA4 was probably the result of a combination of several factors, illustrated in three schematic drawings in Fig. 16. Following deposition of FA3 (Fig. 16A), the onset of sedimentation of FA4 was caused by gravitational sliding of UG cycle 7 (Fig. 16B and C). Steep local slopes and newly created topography caused rapid sedimentation into the topographic lows, sourced from nearby FA3 sediments on topographic highs. Due to the pace of sedimentation and the slope instability, the sediment was in a weakened state and under the influence of continued increasing overburden pressure; some of these weak sediment beds formed convolute lamination. Both the initial gravitational sliding of gypsum on the regional slope as well as the deformation of weakened sediment beds were the result of increased overburden pressure due to a rise in sea level.

The transition to the marine Trubi Formation (FA5). The change to mud-dominated FA5 indicates the demise of the sediment source that fed the Arenazzolo Formation. The abrupt boundary with the Trubi Formation, characterized by pervasive burrowing, indicates a further transgression, strong change in sediment source and the rapid invasion of burrowing organisms. This specific transition likely resulted from the sudden change to deep (open) marine environments caused by concurring palaeoceanographic changes at Gibraltar that installed the modern two-way exchange pattern of Mediterranean–Atlantic connectivity at the base of the Zanclean. Any evidence for a major erosional unconformity between the Arenazzolo Formation and Trubi Formation as was previously postulated by Clauzon *et al.* (1996) was not observed. Moreover, an erosional unconformity at the base of the Arenazzolo Formation that Clauzon *et al.* (2005) correlate to the MES also was not observed.

Current results are also difficult to reconcile with the interpretation of Bache *et al.* (2012) that the Arenazzolo Formation comprises 6.5 precession cycles reflected by dark–light alternations. In the first place, such dark–light alternations have not been observed in the field. Second,

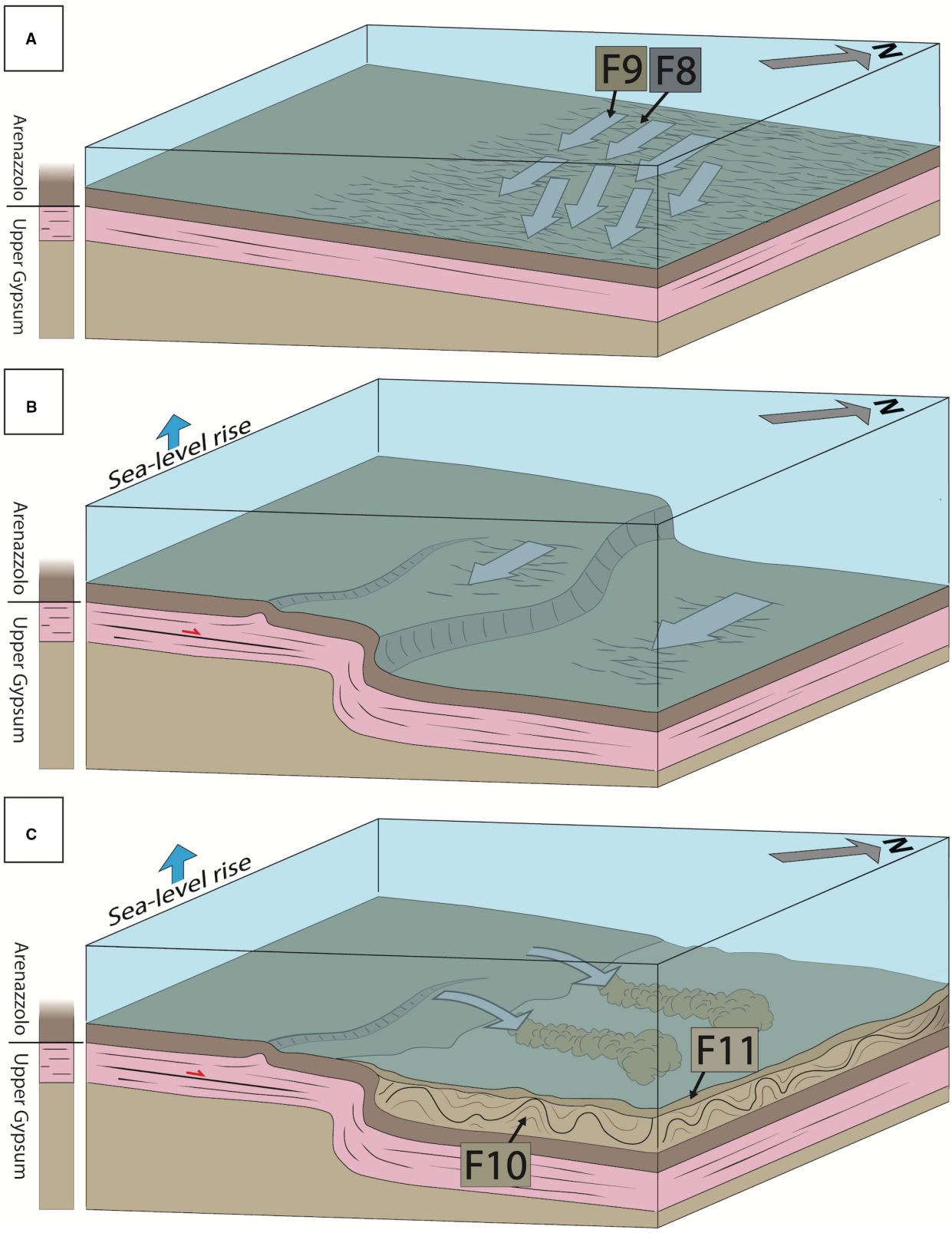

Fig. 16. Schematic model for deposition of FA3 and FA4. (A) Deposition of FA3 (F8 and F9), characterized by along-slope currents. (B) Evolution of the folded Upper Gypsum sequence formed under the influence of increasing overburden pressure due to a rising water column. (C) Envisioned sedimentary environment of FA4 (F10 and F11) with sediment transport from the nearby topographic highs towards the newly formed topographic lows.

there is no independent calibration for such a cyclostratigraphic interpretation based on other dating techniques. Third, and most importantly, present observations imply recurring phases of deposition and erosion (FA3) interrupted by sudden gypsum deformation affecting sedimentation (FA4), which is in conflict with the stable and quiet depositional conditions required to record precession cycles.

Palaeogeographical reconstruction of the Arenazzolo Formation

All observations indicate that the Arenazzolo Formation formed in a transgressive submarine environment exposed to a strong contour parallel current. A rise in sea level potentially connected previously disconnected fold and thrust belt basins generating a strong current flowing east to south-eastward, along the slope. Two options for the origin of such a current are hypothesized in Fig. 15B. Firstly, a current could have originated in the west (Adventure Bank), overtopping a local high formed by the Gela thrust front, directed towards the south-east and enhanced by the local physiography formed by the curved Gela thrust front. Alternatively, the current might have been generated by the establishment of a connection between the formerly disconnected Belice Basin (wedge-top) and Caltanissetta Basin creating a strong bottom current, flowing through a Belice – Caltanissetta gateway, parallel to the Gela thrust front. In both scenarios, previously nearby deltas that delivered UG sandstones were drowned due to the increase in base level.

THE 'TERMINAL MESSINIAN FLOOD' OF THE MEDITERRANEAN

A genetic link between the Arenazzolo Formation and Mediterranean flooding?

The theory of a Zanclean Flood generally implies a significant drawdown of the Mediterranean (1750 to 1900 m lower compared to modern-day levels), with a relatively abrupt end of the crisis generating a Mediterranean-wide flood of unprecedented discharge (Garcia-Castellanos *et al.*, 2009; Micallef *et al.*, 2018; Spatola *et al.*, 2020; Amarathunga *et al.*, 2022). In this scenario, the Sicily Sill is the easternmost barrier of the terminal flood coming in from the Atlantic. After overcoming the barrier of the Gibraltar strait, the western Mediterranean refills until it reaches the level of the Sicily Sill (see Figs 15B and 17). Next, it overtops this sill and establishes a strong eastward current that links the western and eastern Mediterranean, terminating on the eastern border of the Malta Escarpment (Fig. 17). It is exactly at this escarpment that a thick chaotic depositional body is present in the seismic profiles, which was earlier linked to the flooding event (Micallef *et al.*, 2018).

The Sicilian Caltanissetta Basin and the Gela Foredeep are the best candidates for gateways connecting the eastern and western Mediterranean. The present-day structural low around the Catania Plain only experienced significant subsidence during the late Pliocene (Micallef *et al.*, 2016), and does not bear any evidence for being a depocentre at the end of the Messinian. In addition, the main activity of the Sicily Rift Zone (Fig. 17), south of the Messinian foredeep basins also post-dates the Messinian (Civile *et al.*, 2010). Thus, the present hypothesis of a current flowing contour-parallel to the basin physiography of the Sicilian fold-and-thrust belt and continuing its way south of the Hyblean Plateau (where Messinian evaporites are relatively thick; Micallef *et al.*, 2018), eventually terminating in the Noto Canyon, seems plausible.

Age and duration of the flooding event

The preferred scenario presented here implies that just prior to Atlantic–Mediterranean reflooding, the western and eastern Mediterranean were disconnected (Garcia-Castellanos *et al.*, 2020; Amarathunga *et al.*, 2022; Andreetto *et al.*, 2022a). One remaining question concerns the timing and duration of the actual flooding event. Two age constraints are available: The top of UG cycle 7 which has an astronomically tuned age of *ca* 5.345 Ma (Andreetto *et al.*, 2022a) and the base of the Trubi Formation which is dated at 5.333 Ma (Hilgen *et al.*, 2007), leaving *ca* 12 kyr between the top of UG cycle 7 and the Trubi Formation. Model calculations of the Zanclean Flood by Garcia-Castellanos *et al.* (2009) suggest a long first period of very little incision at Gibraltar (possibly several thousands of years) and an exponential increase in incision rate and water flow thereafter. Before the western Mediterranean water level reached the Sicily Sill, flow rates slowed down again due to the reduction in hydrological gradient. It is somewhere between this slowdown of the infill of the western Mediterranean and the full reestablishment of marine conditions of the entire Mediterranean that the

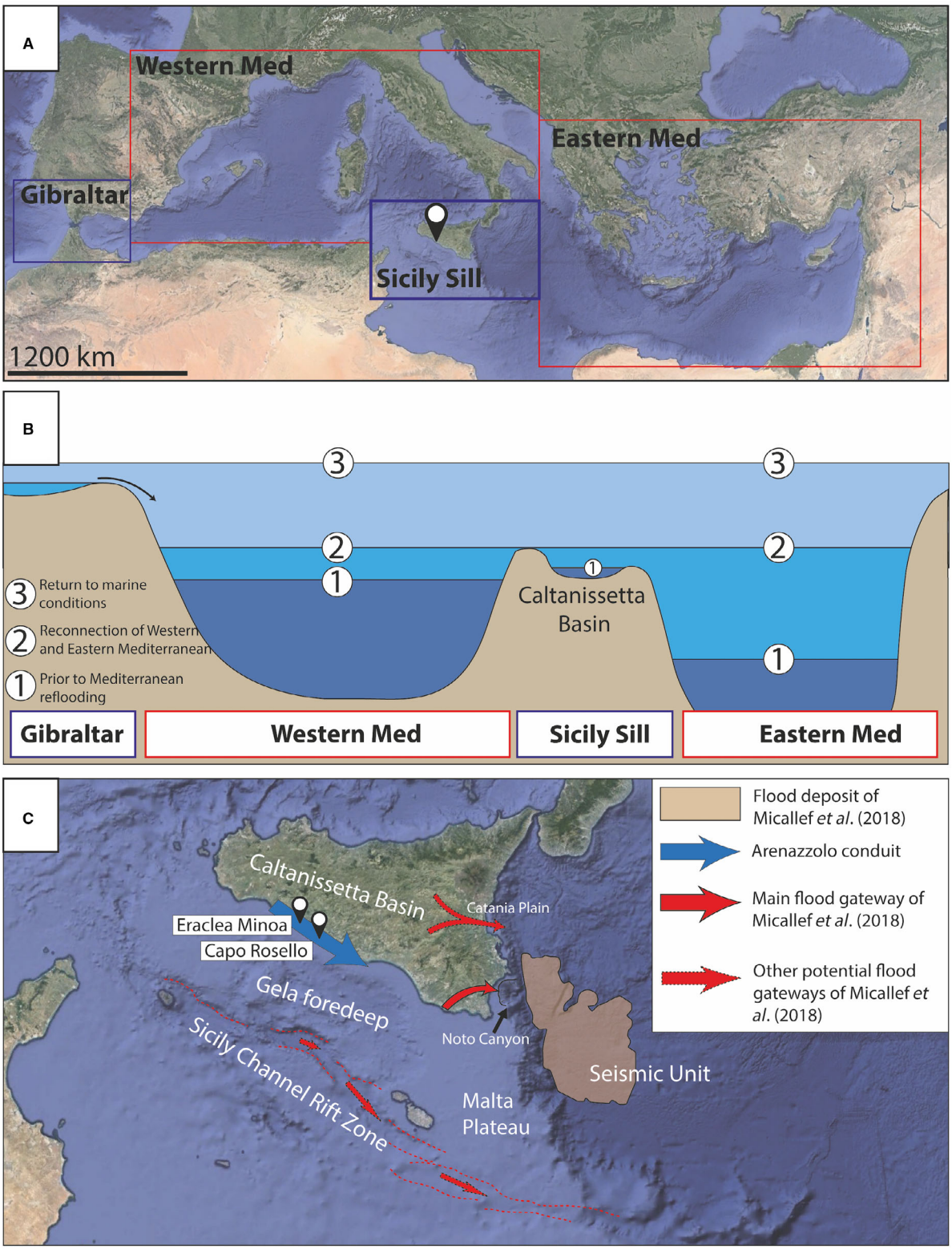

Fig. 17. Potential relationship between the Arenazzolo Formation and the Mediterranean reflooding. (A) Four main sectors of the Mediterranean relevant for this scenario; Gibraltar strait, Western Mediterranean, Sicily Sill and Eastern Mediterranean. (B) Schematic bathymetry for these four different sectors, and three stages of base-level during the Mediterranean reflooding (1 to 3). (C) Map depicting the potential routes of currents during the Mediterranean reflooding (from bathymetry 1 to 2 in B).

Arenazzolo Formation was deposited. Following the model calculations of Garcia-Castellanos *et al.* (2009), a time window for Arenazzolo Formation deposition of a few hundreds of days is assumed (see fig. 3 in Garcia-Castellanos *et al.*, 2009). Given the uninterrupted accretion of sand throughout the Arenazzolo Formation, and the evidence for high sedimentation rate and high flow rate this seems plausible. It leaves *ca* 12 kyr for deposition of the clays between the top UG cycle 7 and the base Arenazzolo Formation, meaning an approximate sedimentation rate of a few tens of centimetres per thousand years, which is reasonable for a mud-dominated prodelta environment, affected by erosion.

Some studies have concluded that there is a need for multiple Mediterranean-wide events of oscillating high-amplitude base level change during the latest Messinian (Rouchy & Caruso, 2006; Andreetto *et al.*, 2022a). This is mainly based on the similarity of the UG on Sicily and Cyprus in the eastern Mediterranean, which also comprise six to seven gypsum–marl couplets (Rouchy *et al.*, 2001). If the scenario of multiple events of connecting and disconnecting the western and eastern Mediterranean basins is correct, an open question remains as to how earlier incursions of western Mediterranean waters into the eastern basin had not triggered a similar depositional unit as the Arenazzolo Formation in the Caltanissetta Basin.

The official base of the Zanclean, the Global Stratotype Section and Point (GSSP) of the Zanclean Stage, that is the Messinian/Zanclean boundary, has been defined at the base of the Trubi Formation at the Eraclea Minoa section (Van Couvering *et al.*, 2000). Following this definition and following this study's palaeoenvironmental interpretation of the Arenazzolo Formation, the Mediterranean flooding did exclusively take place in the latest Messinian and the entire Mediterranean was filled at the base of the Zanclean. In that respect, the authors propose to term the Mediterranean flooding 'Terminal Messinian Flood' to better reflect the temporal evolution of this remarkable event.

CONCLUSIONS

Present work offers new insights into the nature of the flood ending the Messinian Salinity Crisis. Prior to the flooding, sandstones in the Sicilian Upper Gypsum unit (Facies Association 1 and Facies Association 2) were deposited between the delta front and the distal prodelta of a local delta sourced from the basin margin. These Upper Gypsum deposits contrast with the overlying Arenazzolo Formation, which is notably different in terms of lithofacies, microfacies, grain-size distribution and overall composition. Observations suggest that the Arenazzolo Formation is the result of a persistent current, fluctuating in strength and directed east to south-eastward, parallel to the regional slope, outside the reach of the local deltas that fed the Upper Gypsum sandstones. This current was interrupted by the sudden development of gravitational sliding of Upper Gypsum cycle 7, creating a topography that focussed rapid deposition into a low. Deformation of gypsum and sand during this final phase of the Arenazzolo Formation deposition resulted from an increased overburden pressure caused by a sudden rise in sea level.

This study proposes a palaeogeographical model that combines the depositional nature of the Arenazzolo Formation, the expected physiography of the Sicilian fold-and-thrust belt during the late Miocene and reported seismic evidence of the impact of a Mediterranean reflooding on the Sicily area. In this model, the Arenazzolo Formation was part of a contouritic drift in between an overtopping western Mediterranean and a rapidly refilling eastern Mediterranean. For the first time, potential onshore evidence is provided for a terminal Messinian flood. This can be used as ground-truth data to calibrate current models of its impact and hydrodynamics. Furthermore, it can serve to improve understanding of contourite deposition in gateways that reconnect formerly isolated basins.

ACKNOWLEDGEMENTS

This research was supported by the project SALTGIANT - Understanding the Mediterranean Salt Giant, a European project which has received funding from the European Union's Horizon 2020 research and innovation program, under the Marie Sklodowska-Curie (grant agreement No 765256). Our sincere thanks go to Leonard Bik and Coen Mulder of Utrecht University for technical support in thin section preparation and grain-size analysis. We would like to thank Associate Editor Dr Adam McArthur and the two anonymous reviewers for their positive and constructive comments that helped us improve the manuscript.

CONFLICT OF INTEREST

The authors declare that they have no affiliations with or involvement in any organization or entity with financial or non-financial interest in the work submitted.

DATA AVAILABILITY STATEMENT

The data that support the findings of this study are available from the corresponding author upon reasonable request.

REFERENCES

Amarathunga, U., **Hogg, A.M.**, **Rohling, E.J.**, **Roberts, A.P.**, **Grant, K.M.**, **Heslop, D.**, **Hu, P.**, **Liebrand, D.**, **Westerhold, T.**, **Zhao, X.** and **Gilmore, S.** (2022) Sill-controlled salinity contrasts followed post-Messinian flooding of the Mediterranean. *Nat. Geosci.*, **15**, 720–725.

Andreetto, F., **Aloisi, G.**, **Raad, F.**, **Heida, H.**, **Flecker, R.**, **Agiadi, K.**, **Lofi, J.**, **Blondel, S.**, **Bulian, F.**, **Camerlenghi, A.**, **Caruso, A.**, **Ebner, R.**, **Garcia-Castellanos, D.**, **Gaullier, V.**, **Laetitia, G.**, **Gvirtzman, Z.**, **Hoyle, T.**, **Meijer, P.T.**, **Moneron, J.** and **Krijgsman, W.** (2021) Freshening of the Mediterranean salt Giant: controversies and certainties around the terminal (upper gypsum and Lago-Mare) phases of the Messinian salinity crisis. *Earth Sci. Rev.*, **216**, 103577.

Andreetto, F., **Flecker, R.**, **Aloisi, G.**, **Mancini, A.M.**, **Guibourdenche, L.**, **de Villiers, S.** and **Krijgsman, W.** (2022a) High-amplitude water-level fluctuations at the end of the Mediterranean Messinian salinity crisis: implications for gypsum formation, connectivity and global climate. *Earth Planet. Sci. Lett.*, **595**, 117767.

Andreetto, F., **Mancini, A.M.**, **Flecker, R.**, **Gennari, R.**, **Lewis, J.**, **Lozar, F.**, **Natalicchio, M.**, **Sangiorgi, F.**, **Stoica, M.**, **Dela Pierre, F.** and **Krijgsman, W.** (2022b) Multi-proxy investigation of the post-evaporitic succession of the Piedmont Basin (Pollenzo section, NW Italy): a new piece in the stage 3 puzzle of the Messinian salinity crisis. *Palaeogeogr. Palaeoclimatol. Palaeoecol.*, **594**, 110961.

Attenborough, D. (1987) *The First Eden: The Mediterranean World and Man*, 1st edn. BBC Books, Collins, UK.

Bache, F., **Popescu, S.-M.**, **Rabineau, M.**, **Gorini, C.**, **Suc, J.-P.**, **Clauzon, G.**, **Olivet, J.-L.**, **Rubino, J.-L.**, **Melinte-Dobrinescu, M.C.**, **Estrada, F.**, **Londeix, L.**, **Armijo, R.**, **Meyer, B.**, **Jolivet, L.**, **Jouannic, G.**, **Leroux, E.**, **Aslanian, D.**, **Reis, A.T.D.**, **Mocochain, L.**, **Dumurdžanov, N.**, **Zagorchev, I.**, **Lesić, V.**, **Tomić, D.**, **Çağatay, M.N.**, **Brun, J.-P.**, **Sokoutis, D.**, **Csato, I.**, **Ucarkus, G.** and **Çakır, Z.** (2012) A two-step process for the reflooding of the Mediterranean after the Messinian salinity crisis. *Basin Res.*, **24**, 125–153.

Bhattacharya, J.P. (2006) Deltas. In: *Facies Models Revisited* (Eds Posamentier, H.W., Walker, R.G.), *SEPM Society for Sedimentary Geology*. https://doi.org/10.2110/pec.06.84.0237.

Bjørlykke, K. (2015) Introduction to sedimentology. In: *Petroleum Geoscience: From Sedimentary Environments to Rock Physics* (Ed Bjørlykke, K.), pp. 31–90. Springer, Berlin, Heidelberg.

Blott, S.J. and **Pye, K.** (2001) GRADISTAT: a grain size distribution and statistics package for the analysis of unconsolidated sediments. *Earth Surf. Process. Landf.*, **26**, 1237–1248.

Brolsma, M.J. (1978) Quantitative forminiferal analysis and environmental interpretation of the Pliocene and topmost Miocene on the south coast of Sicily. *Utrecht Micropaleontol. Bull.*, **18**, 1–159.

Butler, R.W.H., **Lickorish, W.H.**, **Grasso, M.**, **Pedley, H.M.** and **Ramberti, L.** (1995) Tectonics and sequence stratigraphy in Messinian basins, Sicily: constraints on the initiation and termination of the Mediterranean salinity crisis. *GSA Bull.*, **107**, 425–439.

Butler, R.W.H., **Maniscalco, R.**, **Sturiale, G.** and **Grasso, M.** (2015) Stratigraphic variations control deformation patterns in evaporite basins: Messinian examples, onshore and offshore Sicily (Italy). *J. Geol. Soc. London*, **172**, 113–124.

Caruso, A., **Blanc-Valleron, M.-M.**, **Da Prato, S.**, **Pierre, C.** and **Rouchy, J.M.** (2020) The late Messinian "Lago-Mare" event and the Zanclean reflooding in the Mediterranean Sea: new insights from the Cuevas del Almanzora section (Vera Basin, south-eastern Spain). *Earth Sci. Rev.*, **200**, 102993.

Catalano, R., **Di Stefano, P.**, **Sulli, A.** and **Vitale, F.P.** (1996) Paleogeography and structure of the Central Mediterranean: Sicily and its offshore area. *Tectonophysics*, **260**, 291–323.

Catalano, R., **Valenti, V.**, **Albanese, C.**, **Accaino, F.**, **Sulli, A.**, **Tinivella, U.**, **Morticelli, M.G.**, **Zanolla, C.** and **Giustiniani, M.** (2013) Sicily's fold–thrust belt and slab roll-back: the SI.RI.PRO. Seismic crustal transect. *J. Geol. Soc. London*, **170**, 451–464.

Chang, A.S. and **Grimm, K.A.** (1999) Speckled beds; distinctive gravity-flow deposits in finely laminated diatomaceous sediments, Miocene Monterey formation, California. *J. Sediment. Res.*, **69**, 122–134.

Cita, M.B. and **Colombo, L.** (1979) Sedimentation in the latest Messinian at capo Rossello (Sicily). *Sedimentology*, **26**, 497–522.

Civile, D., **Lodolo, E.**, **Accettella, D.**, **Geletti, R.**, **Ben-Avraham, Z.**, **Deponte, M.**, **Facchin, L.**, **Ramella, R.** and **Romeo, R.** (2010) The Pantelleria graben (Sicily Channel, Central Mediterranean): an example of intraplate 'passive' rift. *Tectonophysics*, **490**, 173–183.

Clauzon, G., **Suc, J.-P.**, **Gautier, F.**, **Berger, A.** and **Loutre, M.-F.** (1996) Alternate interpretation of the Messinian salinity crisis: controversy resolved? *Geology*, **24**, 363–366.

Clauzon, G., **Suc, J.-P.**, **Popescu, S.-M.**, **Marunteanu, M.**, **Rubino, J.-L.**, **Marinescu, F.** and **Melinte, M.C.** (2005) Influence of Mediterranean Sea-level changes on the Dacic Basin (Eastern Paratethys) during the late Neogene: the Mediterranean Lago Mare facies deciphered. *Basin Res.*, **17**, 437–462.

DeCelles, P.G., **Langford, R.P.** and **Schwartz, R.K.** (1983) Two new methods of paleocurrent determination from trough cross-stratification. *J. Sediment. Res.*, **53**, 629–642.

Decima, A. and **Wezel, F.** (1973) Late Miocene evaporites of the central Sicilian Basin, Italy. *Init. Rep. Deep Sea Drilling Proj.*, **13**, 1234–1239.

Duermeijer, C.E. and **Langereis, C.G.** (1998) Astronomical dating of a tectonic rotation on Sicily and consequences for the timing and extent of a middle Pliocene deformation phase. *Tectonophysics*, **298**, 243–258.

Esentia, I., **Stow, D.** and **Smillie, Z.** (2018) Contourite drifts and associated bedforms. In: *Submarine Geomorphology, Springer Geology* (Eds Micallef, A., Krastel, S. and Savini, A.), pp. 301–331. Springer International Publishing, Cham.

Folk, R.L. and **Ward, W.C.** (1957) Brazos River bar [Texas]; a study in the significance of grain size parameters. *J. Sediment. Res.*, **27**, 3–26.

Garcia-Castellanos, D., **Estrada, F.**, **Jiménez-Munt, I.**, **Gorini, C.**, **Fernàndez, M.**, **Vergés, J.** and **De Vicente, R.** (2009) Catastrophic flood of the Mediterranean after the Messinian salinity crisis. *Nature*, **462**, 778–781.

Garcia-Castellanos, D., **Micallef, A.**, **Estrada, F.**, **Camerlenghi, A.**, **Ercilla, G.**, **Periáñez, R.** and **Abril, J.M.** (2020) The Zanclean megaflood of the Mediterranean – searching for independent evidence. *Earth Sci. Rev.*, **201**, 103061.

García-Veigas, J., **Cendón, D.I.**, **Gibert, L.**, **Lowenstein, T.K.** and **Artiaga, D.** (2018) Geochemical indicators in Western Mediterranean Messinian evaporites: implications for the salinity crisis. *Mar. Geol.*, **403**, 197–214.

Gliozzi, E., **Ceci, M.E.**, **Grossi, F.** and **Ligios, S.** (2007) Paratethyan ostracod immigrants in Italy during the late Miocene. *Geobios*, **40**, 325–337.

Gonthier, E.G., **Faugères, J.-C.** and **Stow, D.a.V.** (1984) Contourite facies of the Faro drift, gulf of Cadiz. *Geol. Soc. Lond. Spec. Publ.*, **15**, 275–292.

Grothe, A., **Sangiorgi, F.**, **Brinkhuis, H.**, **Stoica, M.** and **Krijgsman, W.** (2018) Migration of the dinoflagellate Galeacysta etrusca and its implications for the Messinian salinity crisis. *Newsl. Stratigr.*, **51**, 73–91.

Haq, B., **Gorini, C.**, **Baur, J.**, **Moneron, J.** and **Rubino, J.-L.** (2020) Deep Mediterranean's Messinian evaporite giant: how much salt? *Global Planet. Change*, **184**, 103052.

Hilgen, F.J., **Kuiper, K.F.**, **Krijgsman, W.**, **Snel, E.** and **van der Laan, E.** (2007) Astronomical tuning as the basis for high resolution chronostratigraphy: the intricate history of the Messinian salinity crisis. *Newsl. Stratigr.*, **4**, 231–238.

Hsü, K.J. (1972) Origin of saline giants: a critical review after the discovery of the Mediterranean evaporite. *Earth Sci. Rev.*, **8**, 371–396.

Hsü, K.J., **Ryan, W.** and **Cita, M.** (1973) Late Miocene desiccation of the Mediterranean. *Nature*, **242**, 240–244.

Krijgsman, W., **Hilgen, F.J.**, **Raffi, I.**, **Sierro, F.J.** and **Wilson, D.S.** (1999) Chronology, causes and progression of the Messinian salinity crisis. *Nature*, **400**, 652–655.

Krumbein, W.C. and **Pettijohn, F.J.** (1938) *Manual of Sedimentary Petrography*. Appleton Century Crofts, New York, NY.

Kuenen, P.H. (1953) Significant features of graded bedding. *AAPG Bull.*, **37**, 1044–1066.

van der Laan, E., **Snel, E.**, **de Kaenel, E.**, **Hilgen, F.J.** and **Krijgsman, W.** (2006) No major deglaciation across the Miocene-Pliocene boundary: integrated stratigraphy and astronomical tuning of the Loulja sections (Bou Regreg area, NW Morocco). *Paleoceanography*, **21**, 1–27. https://doi.org/10.1029/2005PA001193.

Lickorish, W.H., **Grasso, M.**, **Butler, R.W.H.**, **Argnani, A.** and **Maniscalco, R.** (1999) Structural styles and regional tectonic setting of the "Gela nappe" and frontal part of the Maghrebian thrust belt in Sicily. *Tectonics*, **18**, 655–668.

Londeix, L., **Benzakour, M.**, **Suc, J.-P.** and **Turon, J.-L.** (2007) Messinian palaeoenvironments and hydrology in Sicily (Italy): the dinoflagellate cyst record. *Geobios*, **40**, 233–250.

Lugli, S., **Vinicio, M.**, **Marco, R.** and **Charlotte, S.B.** (2010) The primary lower gypsum in the Mediterranean: a new facies interpretation for the first stage of the Messinian salinity crisis. *Palaeogeogr. Palaeoclimatol. Palaeoecol.*, **297**, 83–99.

Maniscalco, R., **Casciano, C.I.**, **Distefano, S.**, **Grossi, F.** and **Di Stefano, A.** (2019) Facies analysis in the second cycle Messinian evaporites predating the early Pliocene reflooding: the Balza Soletta section (Corvillo Basin, Central Sicily). *Italian J. Geosci.*, **138**, 301–316.

Manzi, V., **Lugli, S.**, **Roveri, M.** and **Schreiber, B.** (2009) A new facies model for the upper gypsum of Sicily (Italy): chronological and palaeoenvironmental constraints for the Messinian salinity crisis in the Mediterranean. *Sedimentology*, **56**, 1937–1960.

Manzi, V., **Roveri, M.**, **Argnani, A.**, **Cowan, D.** and **Lugli, S.** (2021) Large-scale mass-transport deposits recording the collapse of an evaporitic platform during the Messinian salinity crisis (Caltanissetta basin, Sicily). *Sed. Geol.*, **424**, 106003.

Micallef, A., **Georgiopoulou, A.**, **Mountjoy, J.**, **Huvenne, V.A.I.**, **Iacono, C.L.**, **Le Bas, T.**, **Del Carlo, P.** and **Otero, D.C.** (2016) Outer shelf seafloor geomorphology along a carbonate escarpment: the eastern Malta plateau, Mediterranean Sea. *Cont. Shelf Res.*, **131**, 12–27.

Micallef, A., **Camerlenghi, A.**, **Garcia-Castellanos, D.**, **Cunarro Otero, D.**, **Gutscher, M.-A.**, **Barreca, G.**, **Spatola, D.**, **Facchin, L.**, **Geletti, R.**, **Krastel, S.**, **Gross, F.** and **Urlaub, M.** (2018) Evidence of the Zanclean megaflood in the eastern Mediterranean Basin. *Sci. Rep.*, **8**, 1078.

Middleton, G.V. (2003) Convolute lamination. In: *Encyclopedia of Sediments and Sedimentary Rocks* (Eds Middleton, G.V., Church, M.J., Coniglio, M., Hardie, L.A. and Longstaffe, F.J.), p. 168. Springer Netherlands, Dordrecht.

Mutti, E. and **Carminati, M.** (2012) Deep-water sands in the Brazilian offshore basins: AAPGSearch and Discovery article 30219. Available at: http://www.searchanddiscovery.com/documents/2012/30219mutti/ndx_mutti.pdf.

Mutti, E., **Tinterri, R.**, **di Biase, D.**, **Fava, L.**, **Mavilla, N.**, **Angella, S.** and **Calabrese, L.** (2000) Delta front associations of ancient flood-dominated fluvio-deltaic systems. *Rev. Soc. Geol. Esp.*, **13**, 165–190.

Ochoa, D., **Sierro, F.J.**, **Lofi, J.**, **Maillard, A.**, **Flores, J.-A.** and **Suárez, M.** (2015) Synchronous onset of the Messinian evaporite precipitation: first Mediterranean offshore evidence. *Earth Planet. Sci. Lett.*, **427**, 112–124.

Ogniben, L. (1957) Secondary gypsum of the Sulphur series, Sicily, and the so-called integration. *J. Sediment. Res.*, **27**, 64–79.

Owen, G. and **Moretti, M.** (2011) Identifying triggers for liquefaction-induced soft-sediment deformation in sands. *Sed. Geol.*, **235**, 141–147.

Popescu, S., **Dalesme, F.**, **Jouannic, G.**, **Escarguel, G.**, **Head, M.J.**, **Melinte-Dobrinescu, M.C.**, **Sütö-Szentai, M.**, **Bakrac, K.**, **Clauzon, G.** and **Suc, J.** (2009) Galeacysta etrusca complex: dinoflagellate cyst marker of paratethyan influxes to the Mediterranean Sea before and after the peak of the messinian salinity crisis. *Palynology*, **33**, 105–134.

Popescu, S.-M., **Cavazza, W.**, **Suc, J.-P.**, **Melinte-Dobrinescu, M.C.**, **Barhoun, N.** and **Gorini, C.** (2021) Pre-Zanclean end of the Messinian salinity crisis: new evidence from Central Mediterranean reference sections. *J. Geol. Soc. London*, **178**, 1–16. https://doi.org/10.1144/jgs2020-183.

Raad, F., **Lofi, J.**, **Maillard, A.**, **Tzevahirtzian, A.** and **Caruso, A.** (2021) The Messinian salinity crisis deposits in

the Balearic promontory: an undeformed analog of the MSC Sicilian basins? *Mar. Petrol. Geol.*, **124**, 104777.

Rebesco, M., **Hernández-Molina, F.J.**, **Van Rooij, D.** and **Wåhlin, A.** (2014) Contourites and associated sediments controlled by deep-water circulation processes: state-of-the-art and future considerations. *Mar. Geol.*, **352**, 111–154.

Rouchy, J.M. and **Caruso, A.** (2006) The Messinian salinity crisis in the Mediterranean basin: a reassessment of the data and an integrated scenario. *Sed. Geol.*, **188–189**, 35–67.

Rouchy, J.M., **Orszag-Sperber, F.**, **Blanc-Valleron, M.-M.**, **Pierre, C.**, **Rivière, M.**, **Combourieu-Nebout, N.** and **Panayides, I.** (2001) Paleoenvironmental changes at the Messinian–Pliocene boundary in the eastern Mediterranean (southern Cyprus basins): significance of the Messinian Lago-Mare. *Sed. Geol.*, **145**, 93–117.

Roveri, M., **Bertini, A.**, **Stefano, A.D.**, **Gennari, R.**, **Gliozzi, E.**, **Grossi, F.**, **Iaccarino, S.M.**, **Lugli, S.**, **Manzi, V.** and **Taviani, M.** (2008a) A high-resolution stratigraphic framework for the latest Messinian events in the Mediterranean area. *Stratigraphy*, **5**, 323–342.

Roveri, M., **Lugli, S.**, **Manzi, V.** and **Schreiber, B.C.** (2008b) The Messinian Sicilian stratigraphy revisited: new insights for the Messinian salinity crisis. *Terra Nova*, **20**, 483–488.

Roveri, M., **Flecker, R.**, **Krijgsman, W.**, **Lofi, J.**, **Lugli, S.**, **Manzi, V.**, **Sierro, F.J.**, **Bertini, A.**, **Camerlenghi, A.**, **De Lange, G.**, **Govers, R.**, **Hilgen, F.J.**, **Hübscher, C.**, **Meijer, P.T.** and **Stoica, M.** (2014) The Messinian salinity crisis: past and future of a great challenge for marine sciences. *Mar. Geol.*, **352**, 25–58.

Ryan, W.B.F. (2009) Decoding the Mediterranean salinity crisis. *Sedimentology*, **56**, 95–136.

Schreiber, B.C., **Friedman, G.M.**, **Decima, A.** and **Schreiber, E.** (1976) Depositional environments of upper Miocene (Messinian) evaporite deposits of the Sicilian Basin. *Sedimentology*, **23**, 729–760.

Selli, R. (1960) Il Messiniano Mayer-Eymar 1867. Proposta di un neostratotipo. *Giorn. Geol. Ser.*, **2**, 1.

Shanmugam, G., **Spalding, T.D.** and **Rofheart, D.H.** (1993) Traction structures in deep-marine, bottom-current-reworked sands in the Pliocene and Pleistocene, Gulf of Mexico. *Geology*, **21**, 929–932.

Slingerland, R.L. and **Williams, E.G.** (1979) Paleocurrent analysis in light of trough cross-stratification geometry. *J. Geol.*, **87**, 724–732.

Spatola, D., **del Moral-Erencia, J.D.**, **Micallef, A.**, **Camerlenghi, A.**, **Garcia-Castellanos, D.**, **Gupta, S.**, **Bohorquez, P.**, **Gutscher, M.-A.** and **Bertoni, C.** (2020) A single-stage megaflood at the termination of the Messinian salinity crisis: geophysical and modelling evidence from the eastern Mediterranean Basin. *Mar. Geol.*, **430**, 106337.

Stoica, M., **Krijgsman, W.**, **Fortuin, A.** and **Gliozzi, E.** (2016) Paratethyan ostracods in the Spanish Lago-Mare: more evidence for interbasinal exchange at high Mediterranean Sea level. *Palaeogeogr. Palaeoclimatol. Palaeoecol.*, **441**, 854–870.

Stow, D.A.V., **Hernández-Molina, F.J.**, **Llave, E.**, **Bruno, M.**, **García, M.**, **Díaz del Rio, V.**, **Somoza, L.** and **Brackenridge, R.E.** (2013) The Cadiz Contourite Channel: Sandy contourites, bedforms and dynamic current interaction. *Mar. Geol.*, **343**, 99–114.

Strachan, L.J. and **Alsop, G.I.** (2006) Slump folds as estimators of palaeoslope: a case study from the Fisherstreet slump of county Clare, Ireland. *Basin Res.*, **18**, 451–470.

Van Couvering, J., **Castradori, D.**, **Cita, M.**, **Hilgen, F.** and **Rio, D.** (2000) The base of the Zanclean stage and of the Pliocene series. *Episodes*, **23**, 179–187.

Vasiliev, I., **Mezger, E.M.**, **Lugli, S.**, **Reichart, G.-J.**, **Manzi, V.** and **Roveri, M.** (2017) How dry was the Mediterranean during the Messinian salinity crisis? *Palaeogeogr. Palaeoclimatol. Palaeoecol.*, **471**, 120–133.

Zahn, R., **Comas, M.C.** and **Klaus, A.** (Eds). (1999) Proceedings of the Ocean Drilling Program, 161 scientific results, Proceedings of the Ocean Drilling Program. Ocean Drilling Program. https://doi.org/10.2973/odp.proc.sr.161.1999.

Manuscript received 20 July 2022; revision accepted 6 January 2023

Supporting Information

Additional information may be found in the online version of this article:

Supplementary material S1. Excel sheet 1 contains grain-size data used for Figs 7, 8, and 11.

Supplementary material S2. Excel sheet 2 contains palaeocurrent data.

Appendix S1. Grain-size analysis.

Appendix S2. Methodology for palaeocurrent analysis.

Fig. S1. (A) Schematic illustration of four possible trough geometries and their corresponding trough axis/palaeocurrent directions. (B) All hypothetical trough geometries for different trough axis orientations and a given orientation of a 2D exposure (dashed red line). Numbering of these geometries is used for categorization of photograph A (Fig. S2) and photograph B (Fig. S3).

Fig. S2. Interpretation of photographed section A (location corresponds to ERA in Fig. 13C).

Fig. S3. Interpretation of photographed section B (location corresponds to ERB in Fig. 13C).

Fig. S4. Rose diagrams of photograph A (Fig. S2) and photograph B (Fig. S3).

